SAMM version 1.0: A numerical model for microbial mediated soil aggregate formation.

Moritz Laub[1,2], Sergey Blagodatsky[2,3], Marijn Van de Broek[1], Samuel Schlichenmaier[2], Benjapon Kunlanit[5,6], Johan Six[1], Patma Vityakon[4,5], and Georg Cadisch[2]

[1]Sustainable Agroecosystems group, Department of Environmental Systems Science, Swiss Federal Institute of Technology (ETH Zurich), Universitätstrasse 2, 8092, Zurich, Switzerland
[2]Institute of Agricultural Sciences in the Tropics (Hans-Ruthenberg-Institute), University of Hohenheim, 70599 Stuttgart, Germany
[3]University of Cologne, Terrestrial Ecology Group, Institute of Zoology, Zülpicher Str. 47b, 50674 Cologne, Germany
[4]Department of Soil Science and Environment, Faculty of Agriculture, Khon Kaen University, Khon Kaen, Thailand
[5]Soil Organic Matter Management Research Group, Khon Kaen University, Khon Kaen, Thailand
[6]Department of Agricultural Technology, Faculty of Technology, Mahasarakham University, Maha Sarakham, Thailand

Correspondence: Moritz Laub (moritz.laub@usys.ethz.ch)

Abstract. Maintaining soil organic matter (SOM) is crucial for healthy and productive agricultural soils and requires understanding at the process level, including the role of SOM protection by soil aggregates and the connection between microbial growth and aggregate formation. We developed the Soil Aggregation through Microbial Mediation (SAMM) model, to represent this important connection. The pools of SAMM are fully measurable, and we calibrated and evaluated it against data from a long-term bare-fallow experiment in a tropical sandy soil. This experiment received additions of plant litter of different compositions, which resulted in twice the soil carbon stocks in the best treatment compared to the control (about 8 vs. 4 t C ha^{-1} in 0-15cm soil depth) after 25 years. As hypothesized, the SAMM model effectively represented the microbial growth response after the addition of litter and the subsequent formation and later destabilization of aggregates. The low correlations between different calibrated model parameters (r < 0.5 for all parameters; r > 0.4 for only 4 of 22) showed that SAMM is parsimonious. SAMM was able to capture differences between treatments in soil organic carbon (Nash-Sutcliffe modeling efficiency (EF) of 0.68), microbial nitrogen (EF of 0.24) and litter carbon (EF of 0.80). The amount of carbon within the aggregates (EF of 0.60) and in the free silt and clay fraction (EF of 0.24) was also simulated very well to satisfactory. Our model results suggested that in spite of the sandy soil, up to 50% of carbon stocks were stabilized through aggregate protection mechanisms; and that microbial and physical aggregate formation coexist. A version of the SAMM model without aggregate protection (SAMMnoAgg) initially failed to stabilize soil organic carbon (EF decreased to -3.68) and the simulation of microbial nitrogen worsened (EF of 0.13). By recalibrating SAMMnoAgg, it was possible to partially correct for the lack of aggregate protection by reducing the rate of mineral-attached carbon decomposition by about 85% (EF of 0.68, 0.75 and 0.18 for SOC, litter carbon and microbial nitrogen, respectively). However, the slightly better evaluation statistics of SAMM (e.g., Akaike information criterion of 5351 vs. 5554) suggest that representing aggregate dynamics within SOM models can be beneficial and necessary to understand the mechanism behind SOM dynamics. Our results indicate that current models without aggregate formation partly compensate

for the absence of aggregate protection by lowering the turnover rates of other pools. Thus, they remain suitable options where data on aggregate associated carbon are not available.

1   Introduction

Soil aggregates play a crucial role in the context of soil carbon sequestration because soil organic matter (SOM) that is stabilized in aggregates is a fraction of SOM that is strongly affected by human activities (Six and Paustian, 2014). There is evidence that the particulate organic matter (POM) stored within the aggregates may be the fraction of SOM that saturates the least if carbon inputs are increased (Castellano et al., 2015), and thus may be a suitable fraction to target for the accumulation of SOM. However, exactly this intra-aggregate POM becomes relatively easily available to decomposers upon disruption of aggregates (Six et al., 2000) and may therefore be considered to be labile. Mineral-associated organic matter (MAOM), on the other hand, is considered to have slower turnover rates, but the pathways upon which it is formed are not completely clear. For example, the concepts of Kallenbach et al. (2016) and Cotrufo et al. (2013) suggest that most of the stable MAOM is of microbial origin, while Angst et al. (2021) recently estimated that about half of MAOM is formed through direct adsorption of dissolved organic matter to soil minerals. As a result, we need a better understanding of the relative importance of the different processes of SOM stabilization, such as MAOM formation and POM protection within aggregates.

Numerical models are a good way to test our mechanistic understanding of complex systems, such as soils, and to improve knowledge of interconnected processes by testing different hypotheses about the system. They allow quantifying fluxes which are not directly measurable and testing one or several conceptual structures of a system against measured data (Necpálová et al., 2015). Thus, they represent an elegant way to test research hypotheses. Despite the existence of conceptual models, the central role of microbial growth in aggregate formation is still incompletely understood and is only poorly represented in current SOM research models that are developed for the field scale. Initial attempts of Segoli et al. (2013), for example, modeled the formation and destruction of micro- and macroaggregates by including a simple microbial activity factor. However, the model was not further developed into an ecosystem model and therefore is only applicable to shorter-term incubation experiments. The Millennial model (Abramoff et al., 2018, 2022) has a specific microbial biomass pool and distinguishes between aggregated and non-aggregated carbon, but its temporal dynamics have not been evaluated against long-term experiments and it does not simulate the effect of nitrogen on the dynamics of SOM.

In the sense of using models to test important research hypotheses, three important concepts/processes related to aggregate formation should therefore be included into models. The first important process is the effect that the composition of the plant residue and the elemental stoichiometry (Sinsabaugh et al., 2013) have on the carbon use efficiency (CUE) of the microbes. It is considered a key factor in stabilizing SOC (Cotrufo et al., 2013). For example, Lavallee et al. (2018) showed that shoot material leads to more stabilized MAOM than root material, which they attributed to a higher CUE for the shoot material due to higher quality (i.e., low C/N and lignin; Cotrufo et al., 2013). Also Laub et al. (2022), in a long-term field experiment, found differences in aggregate dynamics between the additions of different types of litter and suggested that these were the result of different CUE that depended on the composition of the litter. Secondly, the effect of microbial activity on aggregate

formation must be considered. Many studies in the literature have shown the direct link between aggregate dynamics and microbial functioning. For example, Bucka et al. (2019) showed, under incubation conditions, that microbial activity associated with dissolved organic matter and POM formed aggregates rapidly. Third, measurable pools. It has been suggested numerous times that next generation SOM models should model carbon pools that are directly measurable (Segoli et al., 2013; Wang et al., 2013; Wieder et al., 2014). However, when doing so, one should adhere as much as possible to the principle of distinct structural identity (e.g. Oldfield et al., 2018; Wang et al., 2022; de Aguiar et al., 2022). Thus, within an optimal model based on measurable pools, any quantity of carbon should maintain its structural identity until it is subject to an actual molecular change. This means that if carbon transfers from one modeled pool to another, this should correspond not only to a transfer of matter between the pools but also to a chemical or physical reaction (e.g., depolymerization, anabolic microbial growth, or adsorption to minerals). As such, MAOM and POM have been identified as possible modelable pools of relative distinct structural identities (e.g. Segoli et al., 2013; Lavallee et al., 2020) and are commonly accepted as the main building blocks of aggregates (Totsche et al., 2017). Furthermore, they can be derived from established soil fractionation schemes and differ strongly in average turnover times and properties (Lavallee et al., 2020; Schrumpf et al., 2013). It is, while POM consists mostly of undecomposed plant material, stabilized MAOM originates either from microbial residues (Kallenbach et al., 2016; Six et al., 2006) or from dissolved organic matter (Angst et al., 2021).

Here, we present an approach to include all the above-mentioned concepts into a model of **Soil Aggregation** through **Microbial Mediation** (SAMM). SAMM is based on the foundations introduced by mechanistic SOM models, such as simulating measurable fractions and aggregates (Abramoff et al., 2018, 2022; Segoli et al., 2013) and the decomposition of plant-derived carbon to low molecular weight carbon, before consumption by microbes (Tang and Riley, 2015; Wang et al., 2013; Zhang et al., 2021). It enriches these concepts by (i) the central role of microbes in soil aggregate formation and (ii) a consistent structural identity of POM and MAOM within aggregates. We applied the model to simulate data from a long-term SOM formation experiment in a tropical sandy soil in Northeast Thailand, which included inputs of litter of different compositions and a non-amended control. SAMM is tested against measured data of microbial biomass, SOC, and carbon in different soil fractions. To better understand the model and it's uncertainty, a Bayesian calibration of the model parameters is performed. The calibrated model was then used to test three main hypotheses:

1. Simulating the connection between microbial growth and aggregate formation with SAMM helps to quantify the relative importance of different SOM stabilizing processes.

2. Including this connection in SOM models is essential to accurately represent the dynamics of SOM formation. Therefore, a model that explicitly simulates aggregate formation as a result of microbial growth will outperform a model of similar structure that does not include aggregate formation.

3. The dynamics of microbial activity, which are linked to temperature, moisture, and litter composition, help to explain dynamics in aggregate formation. Thus, we expect that aggregates can be simulated with model performance similar to that of microbial biomass.

Table 1. Chemical characteristics of applied organic residues/litter. Total carbon was measured by Walkley and Black wet digestion; total nitrogen by micro-Kjeldahl, lignin and cellulose by acid detergent lignin method (Van Soest and Wine, 1968); polyphenols were determined according to Anderson and Ingram (1993). Values within the same column that share the same capital letter are not significantly different (p < 0.05). The table is adopted from Laub et al. (2022) under the creative common license 4: http://creativecommons.org/licenses/by/4.0/.

Litter type (Abbreviation)		Carbon (g kg^{-1})	Nitrogen (g kg^{-1})	C/N (g g^{-1})	Lignin (g kg^{-1})	Polyphenols (g kg^{-1})	Cellulose (g kg^{-1})
Rice straw	(RS)	367[A]	4.7[A]	78[A]	28.7[A]	6.5[A]	507[A]
Groundnut stover	(GN)	388[A]	22.8[B]	17[B]	67.6[A]	12.9[A]	178[AB]
Dipterocarp	(DP)	453[B]	5.7[A]	80[A]	175.5[B]	64.9[B]	306[AB]
Tamarind	(TM)	427[B]	13.6[C]	32[C]	87.7[C]	31.5[C]	143[B]
SE[+]		7	0.8	3.4	19	5.6	46

[+]Standard error

2 Material and Methods

2.1 Description of the experiment

We tested the capability of SAMM in a long-term bare fallow experiment, which was established on a degraded tropical sandy
90 soil in 1995 (Vityakon et al., 2000; Puttaso et al., 2011, 2013; Laub et al., 2022). In brief, the experiment was initiated to study the effects of annual additions of organic material (at a rate of 10 t dry matter ha^{-1} yr^{-1}) of different compositions on the dynamics of soil organic matter. The experiment is located within the research station of the Office of Agriculture and Cooperatives of the Northeast, Khon Kaen province (16°20' N; 102° 49' E) in Northeast Thailand. The soil is a Khorat sandy loam (Typic Kandiustult in USDA, Acrisol in WRB classification) with 90% sand and 5% clay (Puttaso et al., 2013). At the
95 start of the experiment, the bulk density was 1.45 g cm^{-3}, the pH was 5.5 and the CEC 3.53 cmol kg^{-1} in the 0-15 cm topsoil (Vityakon et al., 2000). Later measurements did not find significant changes in bulk density due to treatments (Fig. A5), so we assumed a constant bulk density of 1.45 g cm^{-3} throughout the whole period for all treatments in this study. The site has a savanna-type climate with a wet period from April to September with approximately 1200 mm annual precipitation and a mean temperature of 28°C (Puttaso et al., 2013). The experiment was a randomized complete block design with three replicated
100 plots of 4 × 4 m size. The annual litter application of 10 t ha^{-1} dry matter at the beginning of the rainy season around May, supplied about 4 t carbon ha^{-1} yr^{-1}. Next to an unamended control (CT), the litter treatments were rice *(Oryza sativa)* straw (RS; high C/N, low lignin/polyphenol contents), groundnut *(Arachis hypogaea)* stover (GN; low C/N, low lignin/polyphenol contents), tamarind *(Tamarindus indica)* litter (TM; medium C/N, medium lignin/polyphenol contents) with leaf/petiole litter ratio of 7:1, and dipterocarp *(Dipterocarpus tuberculatus*; DP; high C/N, high lignin/polyphenol contents) leaf litter (Table 1).
105 The applied litter was manually incorporated into the topsoil to a depth of approximately 15 to 20 cm using hand hoes. Hand weeding was conducted to keep the plots free of vegetation. This was done about once a month during the rainy season and every second month for the rest of the year, attempting to have as little as possible additional organic matter input from weeds.

Table 2. Overview of all measurements from the Khon Kaen long-term experiment that were used in this study.

Type	Unit[*]	Frequency	Weeks[+]	Time span and reference
Litterbag C	kg C ha^{-1}	6 yr^{-1}	0, 2, 4, 8, 16, 32	2004[a]
Microbial N	kg N ha^{-1}	6 yr^{-1}	0, 2, 4, 8, 16, 32	1995[b], 96-99[X], 2004[a], 07[X], 12[X], 19[c]
Soil organic C	kg C ha^{-1}	1 yr^{-1}	0	1995-2005[d], 2006-16[X], 2019[c]
Soil C/N	g g^{-1}	1 yr^{-1}	0	1995-2005[d], 2006-16[X], 2019[c]
Aggregate C	kg C ha^{-1}	6 yr^{-1}	0, 2, 4, 8, 16, 30	2019[c]
Free mineral-associated C	kg C ha^{-1}	6 yr^{-1}	0, 2, 4, 8, 16, 30	2019[c]

[*]Data rescaled to kg ha^{-1} using 15 cm soil depth and a bulk density of 1.45 g cm^{-3}; [+]Weeks after residue addition (0 = prior); References: [a]Puttaso et al. (2011), [b]Vityakon et al. (2000), [c]Laub et al. (2022), [d]Vityakon (2007), [X]Unpublished

However, despite best efforts it was not possible to keep the plots completely free of vegetation at all times. The experimental data covered a time period from the establishment of the experiment in 1995 to December 2019.

2.2 Available long-term experiment data that was simulated with SAMM

Carbon and nitrogen data from soil microbial biomass were available from most years and were always measured prior to the incorporation of litter and at weeks 2, 4, 8, 16 and 32 after the addition of litter (Puttaso et al., 2011; Vityakon et al., 2000; Vityakon, 2007; Laub et al., 2022, and unpublished data in Table 2). Litterbag decomposition experiments were conducted to elucidate differences in litter decomposition rates as a function of litter composition, measuring ash-free dry weight remaining at the same points in time (Puttaso et al., 2011). THe soil microbial biomass was measured by chloroform fumigation extraction (see Puttaso et al., 2011, for more details). Because microbial carbon and nitrogen are usually correlated, we only used microbial nitrogen data, which were of higher quality (fewer negative values than carbon, lower variability within treatments). Annual measurements of soil organic carbon and soil C/N data, measured by the Walkley-Black method (Walkley and Black, 1934), were available from Vityakon et al. (2000) and from additional annual measurements until 2016 and from 2019. Furthermore, there were measurements of carbon in aggregates (carbon in small macroaggregates, 2–0.25 mm; and microaggregates, 0.25–0.053 mm; combined) and the free silt and clay faction (MAOC) throughout the year 2019 at weeks 0, 2, 4, 8, 16 and 30 (Laub et al., 2022).

2.3 The SAMM model version 1.0: Core concepts and model description

The core concepts of SAMM are 1) all pools are measurable entities that adhere to the concept of structural carbon identity (Wang et al., 2022), which they maintain within the aggregates and along the gradient of increased decomposition status, 2) linking the formation of the aggregates with the microbial life cycle, and 3) simulating aggregates in a coupled soil carbon and nitrogen model. For brevity, we only explain the central concepts of SAMM and the flow of carbon and nitrogen in the main
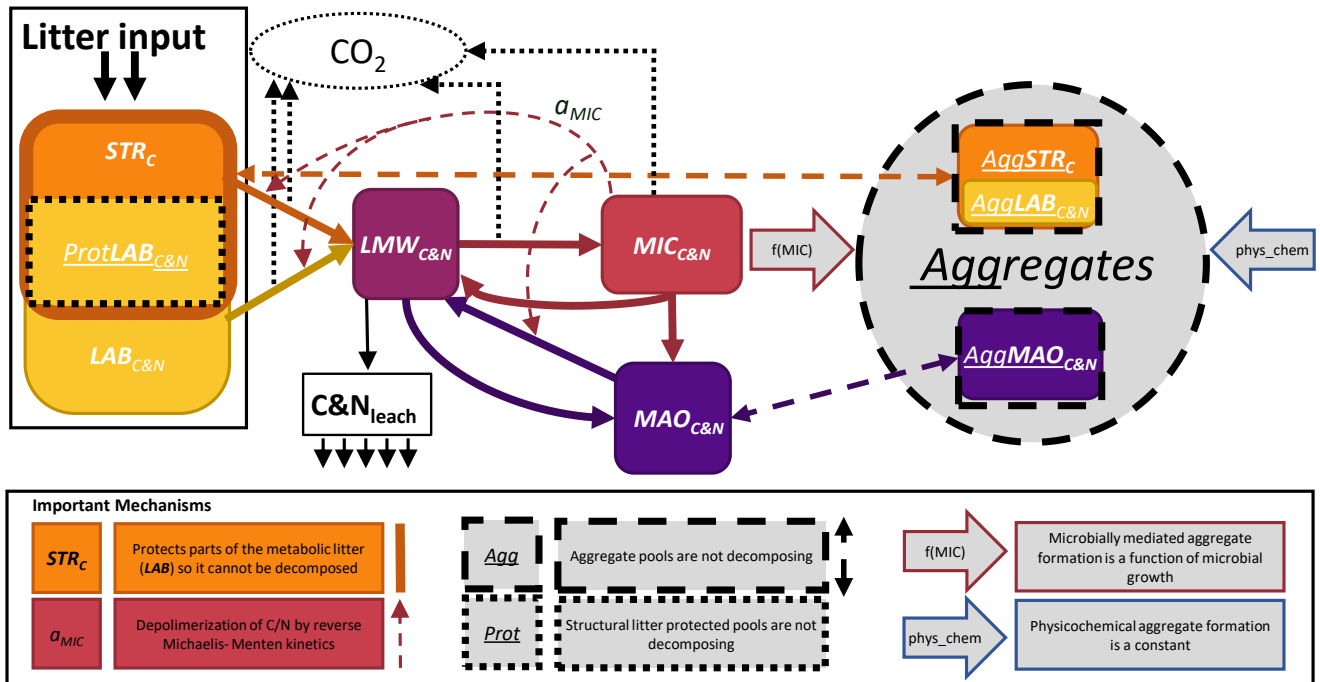
Figure 1. Conceptual model of SAMM. The carbon and nitrogen in the pools are represented as $Pool_{C\&N}$ or $Pool_C$ for the pools only with carbon. The following pools exist: STR_C, structural litter; $LAB_{C\&N}$, labile litter; $LMW_{C\&N}$, low molecular weight; $MIC_{C\&N}$, microbial; $MAO_{C\&N}$, mineral-associated. Thick continuous arrows represent flows of carbon and nitrogen between pools that include a change in structural identity. The thick dashed arrows represent aggregate protection and deprotection, which does not change the structural identity. The effect of $MIC_{C\&N}$ on pool decomposition by reverse Michaelis Menten kinetics (a_{MIC} parameter) is represented by the thin dashed arrow. The two large arrows with a colored outline represent the factors that influence the rate of aggregate formation. Losses from the system are represented by thin dotted arrows (CO_2) and continuous arrows (leaching). Further abbreviations: $Prot$, protected by structural litter; Agg, aggregate protected pools.

text, while the Appendix hosts a detailed description of model pools (A1) and the differential equations comprising the SAMM model (A3). A list of all model pools is given in Table 3, while all parameters and their calibrated values are given in Table 4.

130   To achieve complete measurability, the simulated fresh litter was divided into two pools, structural litter measured as lignin and polyphenols (similar to Campbell et al., 2016), and labile (metabolic) litter representing the carbon and nitrogen of the remaining litter, thus allowing different CUE and decomposition rates resulting in differences in microbial growth. By simulating both carbon and nitrogen, the model further allows for a C/N ratio-dependent CUE at microbial uptake. The carbon and nitrogen cycles are coupled (Fig. 1 and Table 3), but the structural litter pool is defined as a carbon-only pool. This is indicated

135   in the following by the subscripts next to the pool names (i.e., $POOL_C$ for carbon-only, and $POOL_{C\&N}$ for carbon and nitrogen containing pools).

Table 3. An overview of all SAMM model pools and their units.

Pool	Description	Unit[+]
STR_C	Structural litter pool C	kg C ha^{-1}
LAB_C	Metabolic litter pool C	kg C ha^{-1}
LAB_N	Metabolic litter pool N	kg N ha^{-1}
LMW_C	Low molecular weight pool C	kg C ha^{-1}
LMW_N	Low molecular weight pool N	kg N ha^{-1}
MIC_C	Microbial biomass pool C	kg C ha^{-1}
MIC_N	Microbial biomass pool N	kg N ha^{-1}
MAO_C	Mineral-associated C	kg C ha^{-1}
MAO_N	Mineral-associated N	kg N ha^{-1}
$AggSTR_C$	Structural litter pool C protected in aggregates	kg C ha^{-1}
$AggLAB_C$	Metabolic litter pool C protected in aggregates	kg C ha^{-1}
$AggLAB_N$	Metabolic litter pool N protected in aggregates	kg N ha^{-1}
$AggMAO_C$	Mineral-associated C protected in aggregates	kg C ha^{-1}
$AggMAO_N$	Mineral-associated N protected in aggregates	kg N ha^{-1}

[+]For a defined depth interval (here 0-15 cm).

The organic matter decomposition process within the SAMM model starts with undecomposed plant material, consisting of structural litter (STR_C), and the labile/metabolic litter pool ($LAB_{C\&N}$). To distinguish between the cell walls and the interior part of $LAB_{C\&N}$, the STR_C protects part of $LAB_{C\&N}$ from decomposition (*ProtLAB* pool; see Appendix A1), mimicking that part of $LAB_{C\&N}$ is interviewed with STR_C in the cell walls. Upon depolymerization, the carbon and nitrogen of any pool enters the easily soluble low molecular weight ($LMW_{C\&N}$) pool. This $LMW_{C\&N}$ is the only pool that contains molecules that are small enough to be incorporated by the microbial biomass ($MIC_{C\&N}$). Extracellular enzyme production consumes energy, which is indirectly accounted for by a pool-dependent carbon use efficiency (*CUE*), leading to CO_2 respiration in the amount of *(1-CUE)* during the transition from any litter pool to $LMW_{C\&N}$. When the $MIC_{C\&N}$ pool consumes $LMW_{C\&N}$, a portion of the consumed carbon is respired as growth respiration, the rest is used for anabolism. The amount of growth respiration of $MIC_{C\&N}$ depends on a variable stoichiometric CUE, which is a function of the C/N ratio of $LMW_{C\&N}$. $MIC_{C\&N}$ is subject to microbial death and microbes also have maintenance respiration. Parts of death microbes (cell walls) are attached to minerals, creating mineral-associated carbon and nitrogen ($MAO_{C\&N}$), the rest (cell internal content) is transferred back into the $LMW_{C\&N}$ pool. Furthermore, $MIC_{C\&N}$ can immobilize or release N, to maintain their C/N ratio (see Appendix A1.4). Direct adsorption of $LMW_{C\&N}$ to $MAO_{C\&N}$ is also possible. Carbon and nitrogen from the primary constituents (i.e., $LAB_{C\&N}$, STR_C, $MAO_{C\&N}$) get protected by integration into aggregates as a byproduct of microbial growth; i.e., the amount of aggregate formation is a function of microbial growth. There is also a physicochemical aggregate formation, which for simplicity is assumed to be constant in version 1.0 of SAMM. Inside the aggregates, there is no decomposition, a concept proposed by Luo et al. (2017)

as a way to reduce the number of parameters in aggregation models. The carbon of all pools outside of aggregates is subject to decomposition by $MIC_{C\&N}$ following reverse Michaelis-Menten kinetics, a good approximation of enzymatic depolymerization (Abramoff et al., 2022; Tang and Riley, 2019). Thus, the speed of decomposition depends on the amount of substrate and the amount of $MIC_{C\&N}$. Aggregate disruption is simulated as a first-order kinetic process.

2.4 SAMM setup and Bayesian calibration

For the technical implementation of SAMM version 1.0, we used the R programming language (R Core Team, 2020). Details are described in the Appendix A2. As SAMM is a new model, we added a mass balance equation to stop the model with an error message if the mass balance was not closed. Further, most model parameters needed to be calibrated. In addition to typical parameters of a SOM model representing pool turnover, SAMM contains some unique parameters, such as the protection capacity that STR_C exhibits on $LAB_{C\&N}$, the rate of aggregate formation per microbial growth, and the rate of physicochemical aggregate formation (Table 4). Additionally, the amount and composition of carbon and nitrogen entering the soil through plant roots were calibrated parameters. These were necessary because, despite best efforts to keep the experiment completely fallow, it was not possible to completely eliminate plant growth in the plots. Two model parameters were fixed on the basis of the literature. The first uncalibrated parameter was the maximum CUE for LMW_C, which was fixed at 0.6 (Sinsabaugh et al., 2013; Manzoni et al., 2012). The second uncalibrated parameter was c_{SORP}, the maximum sorption capacity of the fine fraction, which was taken from Abramoff et al. (2022). To initialize the pools, we used the mean of the measured SOC fractions in the rice straw treatment in 2019, which had not experienced major changes in SOC since the start of the experiment. In the absence of fractionation data from the start of the experiment' and historic plant input quantities and qualities, this was considered the best option. Ideally, SOC fractions would be measured at the beginning of any experiment. However, sensitivity analyses, perturbing the distribution of initial SOC between MAOC and litter pools from 80 to 120% of our initial assumptions confirmed a very limited effect (any visible differences in simulated SOC and aggregate C disappeared within less than ten and less than three years, respectively; see response to referee comments https://doi.org/10.5194/egusphere-2023-1414-AC1).

To test our hypotheses about the importance of aggregates in carbon stabilization and the need to simulate this process, we also created a SAMM version without aggregate formation (SAMMnoAgg). By setting the turnover of aggregates (k_{Agg}) to 1 d⁻¹ and the aggregate formation parameters to 0, all aggregate protection was effectively removed from the model. We evaluated the difference in simulated stabilized SOC in SAMM and SAMMnoAgg, using the parameters calibrated for SAMM, to gain insight into the importance of aggregate protection for SOC stabilization. SAMMnoAgg was further recalibrated to test our hypothesis of the need to simulate aggregates to represent SOM dynamics. Note that measurements of carbon in aggregates and in silt and clay fractions of 2019 were not used to recalibrate SAMMnoAgg.

As a starting point for the model parameters, an initial model calibration was performed using a genetic algorithm (GA package of R; Scrucca, 2013). To explore the uncertainty associated with the two different versions (i.e., SAMM and SAMMnoAgg), this initial calibration was followed by a Bayesian calibration applying the sampling importance resampling (SIR) method. This method was used by Gurung et al. (2020) to calibrate the SOM module of DayCent and is described in detail in their article. Briefly, the SIR method uses Bayes' theorem to derive the posterior distribution of model parameters and model

Table 4. Overview of all SAMM model parameters (top), further computed helper variables (middle) and external model drivers and site conditions needed (bottom). The calibrated values are the best parameter set from the independent Bayesian calibration for the SAMM model and the recalibrated non aggregate model (SAMMnoAgg).

Variable	Description	Units	Calibrated	SAMM[1]	SAMMnoAgg[2]
k_{STR}	Turnover rate of structural litter pool	g g^{-1} d^{-1}	Yes	0.0024	0.0028
k_{LAB}	Turnover rate of metabolic litter pool	g g^{-1} d^{-1}	Yes	0.0225	0.0551
k_{MIC}	Death rate of microbial biomass pool	g g^{-1} d^{-1}	Yes	0.0046	0.0098
k_{MAO}	Turnover rate of mineral-associated carbon pool	g g^{-1} d^{-1}	Yes	0.00044	0.000057
μ_{max}	Maximum uptake rate of LMW by microbes	g g^{-1} d^{-1}	Yes	0.238	0.367
k_{Agg}	Turnover rate of aggregate pools	g g^{-1} d^{-1}	Yes	0.0316	1[x]
$K_{M_{MIC}}$	Half-saturation constant of the microbial activity factor	-	Yes	35.5	1.0
m_{MIC}	Maintenance respiration of microbes	g g^{-1} d^{-1}	Yes	0.00035	0.0013
K_{LMWMAO}	Specific adsorption rate of LMW to MAOM	g g^{-1} d^{-1}	Yes	0.043	0.031
c_{SORP}	Maximum sorption capacity coefficient	g g^{-1}	No[*]	0.83	0.83
CUE_{STR}	Carbon use efficiency of structural litter pool	g g^{-1}	Yes	0.65	0.52
CUE_{LAB}	Carbon use efficiency of metabolic litter pool	g g^{-1}	Yes	0.54	1.00
CUE_{LMW}	Maximum carbon use efficiency of low molecular weight pool	g g^{-1}	No[+]	0.6	0.6
$CN_{min(MIC)}$	Minimum C/N ratio of microbial biomass pool	g g^{-1}	Yes	5.01	6.12
$CN_{max(MIC)}$	Maximum C/N ratio of microbial biomass pool	g g^{-1}	Yes	10.1	9.49
$f_{MICMAOM}$	Fraction of MIC directed to MAOM upon microbial death	g g^{-1}	Yes	0.24	0.26
$pc_{STR_{LAB}}$	Protection capacity of STR_C for $LAB_{C\&N}$	g g^{-1}	Yes	2.47	3.98
$aggfactSTR_C$	Protection of STR_C inside aggregates per microbial growth	g g^{-1}	Yes	0.71	0[x]
$aggfactMAO_C$	Protection of MAO_C inside aggregates per microbial growth	g g^{-1}	Yes	2.70	0[x]
$NonMicAgg$	Physicochemical aggregate formation	kg MIC_Ceq ha^{-1} d^{-1}	Yes	31.0	0[x]
$DailyLitter_C$	Daily root carbon inputs (from unavoidable plant growth)	kg C ha^{-1} d^{-1}	Yes	3.07	3.09
$DailyLitter_{C/N}$	C/N ratio of daily root inputs	g g^{-1}	Yes	159.3	47.0
$DailyLitter_{STRC(\%)}$	Percent of structural litter in daily root inputs	g g^{-1}	Yes	0.13	0.24
Computed helper variables (rate modifiers etc.)					
$CUE_{CN(LMW)}$	Dynamic C/N based carbon use efficiency of LMW_C pool	g g^{-1}	-	-	-
s_t	Temperature scalar	-	-	-	-
s_w	Water scalar	-	-	-	-
$pLAB$	Fraction of metabolic litter protected by structural litter	g g^{-1}	-	-	-
a_{MIC}	Michaelis-Menten microbial activity factor	-	-	-	-
$MAO_{C_{max}}$	Maximum adsorption capacity to MAO_C	t ha^{-1}	-	-	-
w_{leach}	Share of soil water leached (HYDRUS calculation)	g g^{-1} d^{-1}	-	-	-
Site condition and other model driving variables					
$depth$	Soil depth to be simulated	m	-	-	-
BD	Bulk density	kg m^{-3}	-	-	-
$\%SiCl$	Silt and Clay fraction	%	-	-	-

[1]Model version including soil aggregates; [2]Recalibrated model version without soil aggregates; [*]from Abramoff et al. (2022); [+]established maximum (Sinsabaugh et al., 2013; Manzoni et al., 2012); [x] set to 0/1 in model version without soil aggregates to deactivate them.

output based on assumed prior and available data. We assumed normally distributed broad priors centered around the initial calibrated model parameters, i.e., the mean parameter values from SAMM and SAMMnoAgg, to have the same priors for both

190 (except for the values only calibrated in the aggregate version). To calibrate SAMM and SAMMnoAgg, we used all available data of litterbag C, microbial N, and SOC, while data of aggregate C and free MAOC were only used to calibrate SAMM. In the next step of SIR, the posteriors are derived by filtering the prior using importance weights to sample individual parameter sets from the prior. The importance weights are proportional to the simulation likelihoods (i.e., of observing the data, given the model), which are computed using the data, the simulated values, and the variance-covariance matrices of data (Wallach

195 et al., 2019). As is common practice, we assumed that the covariances were zero, and hence we only used the variances for each type of measurement (taking the median variance computed for each type of data from the three experimental repetitions). Then, by dividing the likelihood of each simulation by the mean likelihood of all simulations, standardized importance weights were computed. The prior parameter set was then resampled without replacement and the importance weights taken as sampling probability. Overall, a total of 200.000 simulations were performed, of which 200 parameter sets were drawn in the

200 resampling.

2.5 Model evaluation

The following standard evaluation statistics were used for model evaluation, as defined by Loague and Green (1991):

$$MSE_y = \frac{1}{n}\sum_{z=1}^{n}(O_{yz} - P_{yz})^2 \tag{1}$$

$$RMSE_y = \sqrt{MSE_y} \tag{2}$$

205 $$EF_y = 1 - \frac{\sum_{z=1}^{n}(O_{yz} - P_{yz})^2}{\sum_{z=1}^{n}(O_{yz} - \bar{O}_y)^2} \tag{3}$$

Here, MSE_y is the mean square error and $RMSE$ is its root. EF_y is the Nash-Sutcliffe modeling efficiency, O_{yz} stands for the measured value of the *z-th* measurement of the *y-th* type of measurement. Furthermore, $\bar{O}_y$ is the mean of measured values of the *y-th* type of measurement and P_{yz} is the model-predicted value corresponding to O_{yz}. As suggested by Gauch et al. (2003) to gain better insight into the nature of model errors, we further divided MSE_y into squared bias (*SB*), nonunity slope (*NU*) and

210 lack of correlation (*LC*). We expressed them in relative terms, by dividing them by MSE_y:

$$SB_y(\%) = \frac{(\bar{O}_y - \bar{P}_y)^2}{MSE_y} * 100 \tag{4}$$

$$NU_y(\%) = \frac{(1 - b_y)^2 * (\frac{\sum_{z=1}^{n}(O_{yz}^2)}{n})}{MSE_y} * 100 \tag{5}$$

10

$$LC_y(\%) = \frac{(1-r_y)^2 * (\frac{\sum_{z=1}^{n}(P_{yz}^2)}{n})}{MSE_y} * 100 \tag{6}$$

Here, $\bar{P}_y$ is the mean predicted value of the *y-th* measurement type, *b* the slope of the regression of *P* on *O*. Finally, *r* is the correlation coefficient between *O* and *P*. The relative *LC*, *SB* and *NU* provide information if the model errors are mostly random (high *LC*) or whether there is a systematic bias (high *SB*). A high relative *NU* indicates that the sensitivity of the model is wrong (either too low or too high). The *SB* can be interpreted as the intercept of a regression between predictions and measured values, while the *NU* is the slope of this regression (Gauch et al., 2003). Finally, the Akaike information criterion (AIC) was computed to compare different model versions:

$$AIC = 2k - 2ln(\bar{L}) \tag{7}$$

Here, *k* is the number of model parameters that were estimated (23 for SAMM and 19 SAMMnoAgg) and $\bar{L}$ is the likelihood.

3 Results

Because SAMM is a new model, we first describe its behavior and illustrate the development of pools (Fig. 2) using the treatment with the highest microbial activity, the groundnut stover treatment. It is important to note that our results cover a time period where the model has not yet reached a new steady state. Second, the performance of the calibrated model is evaluated against the measured data, and posterior parameter distributions are discussed. Third, we test the importance of aggregate protection in SAMM, by assessing how much the simulation performance decreases for different types of measurements when aggregate formation is not simulated (SAMMnoAgg). Finally, we try to assess to which extent simulating aggregate formation is necessary to correctly simulate microbial biomass and SOC, by recalibrating the SAMMnoAgg version and comparing it to SAMM.

3.1 SAMM model behavior: the connection between microbes and aggregate formation

After the groundnut stover application in 2001, a rapid depolymerization of the part of LAB_C that is not protected by STR_C is simulated (Fig. 2). The depolymerized material is transferred to the LMW_C pool. This increase in LMW_C feeds the growth of MIC_C, which almost triples in biomass. The MIC_C growth slows down once the unprotected part of LAB_C is fully decomposed. However, the peak of LMW_C availability is within one to two weeks after litter addition, while the peak of MIC_C is about one to two months after litter addition and maximum LMW_C availability. The increase in microbial growth is accompanied by an increase in the formation of new aggregate-protected carbon. Unprotected MAO_C and litter get thereby protected in aggregates, increasing the amount of aggregate protected MAO_C and litter by approximately 30%. Because the formation of aggregates is linked to microbial growth, the peak of aggregate protected pools (MAO_C, LAB_C and STR_C) occurs simultaneously with the peak of MIC_C. Subsequently, the amount of aggregate carbon starts to reduce again, which becomes visible in the increase
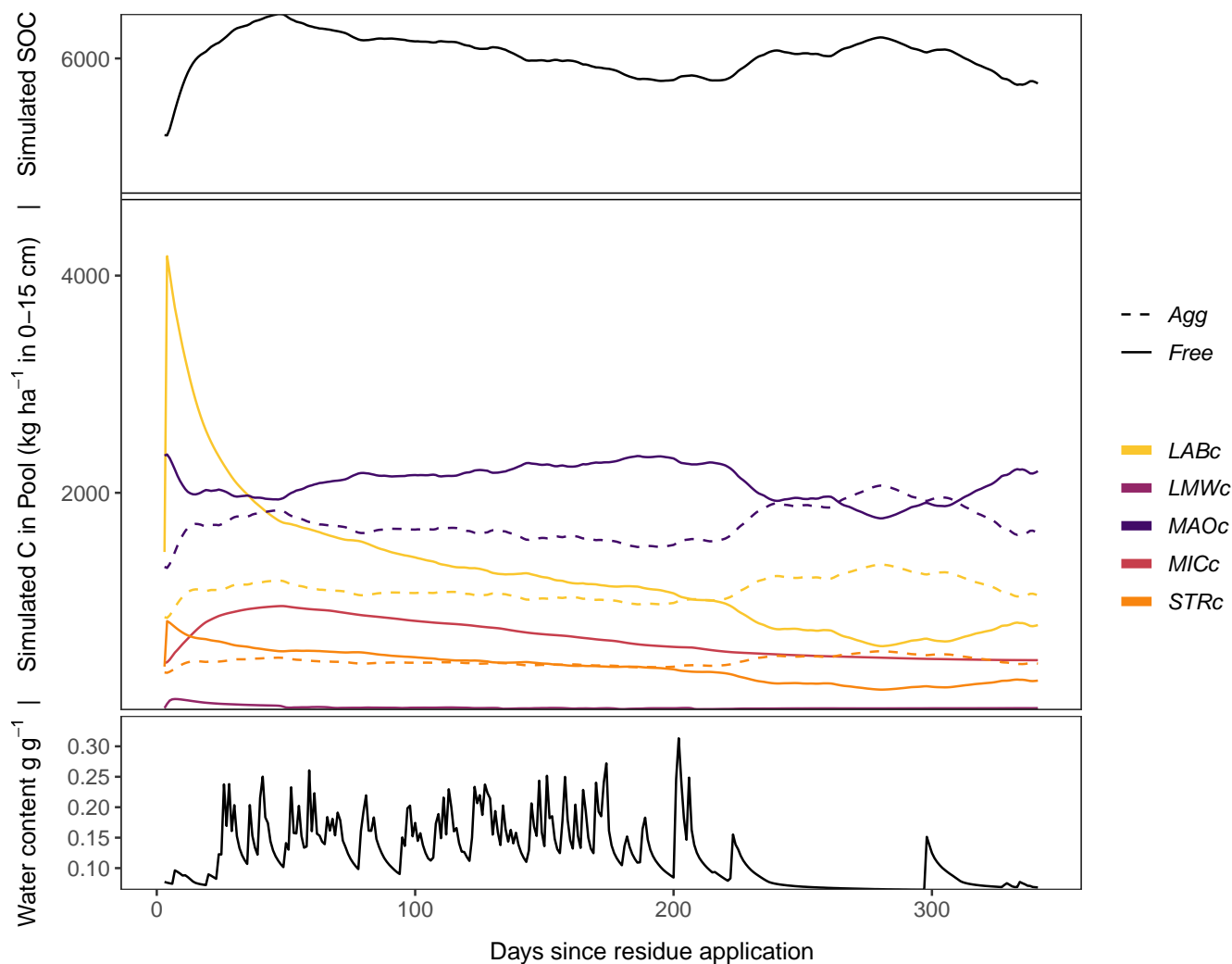
11

Figure 2. Exemplary SAMM model behavior and carbon pool dynamics of the groundnut treatment in the year 2001 to 2002 starting a day before the addition of litter. The top figure displays all carbon pools inside and outside of aggregates, while the bottom figure displays the soil water content (model driver, simulated by HYDRUS 1D). In the two figure, aggregate protected pools (Agg) are represented by a dashed line, decomposable (Free) pools by a solid line. STR_C, structural litter; LAB_C, labile litter; LMW_C, low molecular weight; MIC_C, microbial; MAO_C, mineral-associated.
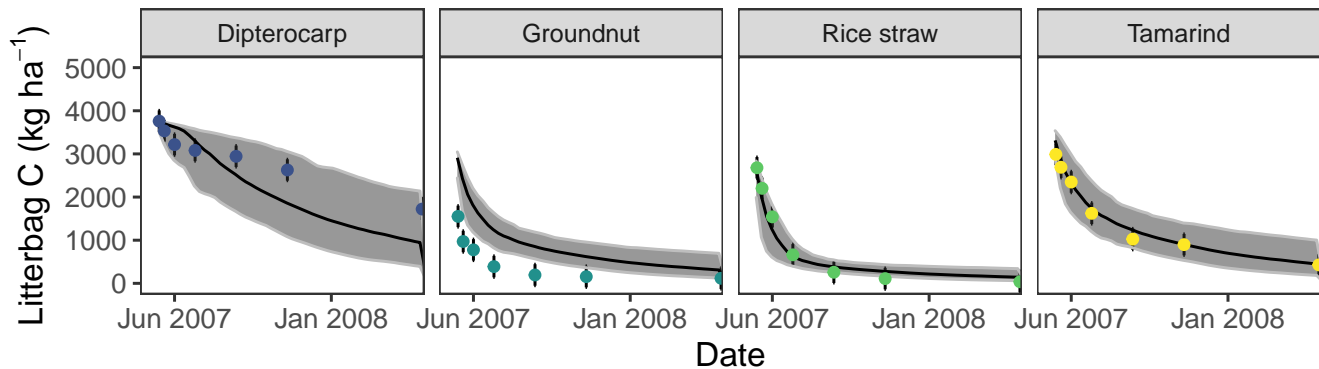
Figure 3. Simulation of incubated litterbag residue-C dynamics from different litter materials (buried at 15 cm depth). Dots with error bars indicate the mean and 95% credibility interval of measured values. The black line and grey band indicate the best simulation and the 95% credibility interval of the Bayesian calibration posterior, respectively.

of unprotected MAO_C, LAB_C and STR_C. During the dry season about 250 days after residue application, another increase in aggregate formation occurs, this time driven by the physicochemical aggregate formation that continues while aggregate turnover is reduced due to limiting water availability. After a full year, just before the next addition of litter, most of the newly added litter of the year before is decomposed and increased moisture availability increases aggregate disruption again.
245 However, a higher amount of MAO_C compared to the beginning of the year and a slightly higher amount of aggregate protected MAO_C, STR_C and LAB_C leads to an increased amount of SOC compared to the previous year.

3.2 Evaluating SAMM against measured data

Overall, the SAMM model was able to simulate the different types of available measurements, as indicated by positive modeling efficiencies for all of them (Table 5a; soil C/N was the only exception). The best representation of the measured values by the
250 model was that of residue-C in litterbags (Fig. 3; EF 0.80) and, interestingly, the measured decomposition of groundnut stover was so fast (>50% in the first week) that the model could not capture it. Furthermore, the measured values of the SOC of the top soil were well represented by SAMM (Fig. 4 and 5; EF 0.68), with a tendency of the model to overestimate SOC in the rice straw treatment and underestimate SOC in the tamarind and groundnut treatments. Further, microbial nitrogen (MIC_N; EF 0.24) and carbon in the free silt and clay fraction (MAO_C; EF 0.24) were simulated with acceptable accuracy (Fig. 5 and
255 6). The temporal trend of microbial nitrogen was also well captured for all litter treatments with the exception of the control, in which there was almost no simulated microbial growth response over the year (Fig. 6). For free MAO_C, the differences between treatments were captured, the temporal dynamic was low, both in measured and modeled values, and the model could overall capture the treatment differences (EF 0.24). It could also very well capture the temporal dynamics of aggregate C in the groundnut, rice straw, and tamarind treatments, as well as the absence of major temporal dynamics in the other two treatments
260 (Fig. 6; EF 0.60). Despite the dynamic CUE function of SAMM, the SOC content of the high C/N ratio residue treatments (rice
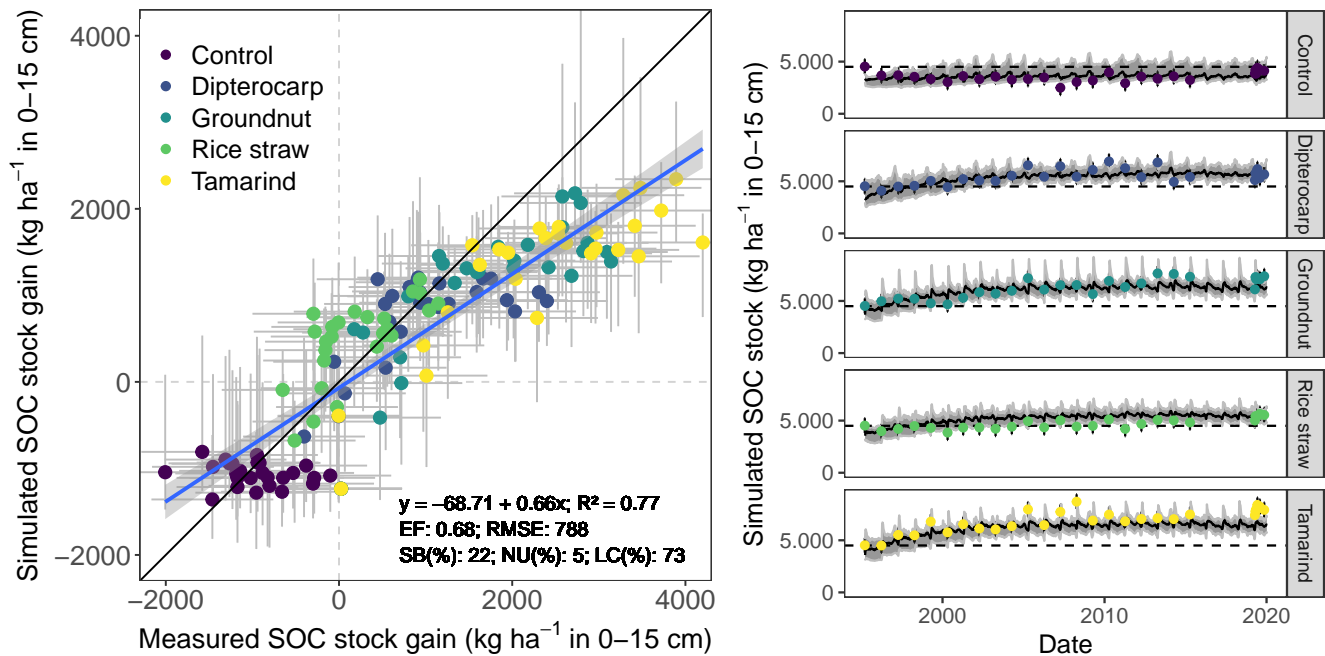
13

Figure 4. Measured and simulated development of SOC stocks in the top 15 cm of soil from all residue addition treatments. Displayed are the measured versus modeled gain in SOC stocks since the onset of the experiment (left), with grey bars indicating 95% credibility interval. Additionally, results for simulated versus measured SOC over time for different residues (right). Dots with error bars indicate the mean and 95% credibility interval of measured values and simulations. The black line and grey band indicate the best simulation and the 95% credibility interval of the Bayesian calibration posterior, respectively.

straw the most strongly and dipterocarp to some extent) tended to be overestimated while tamarind tended to be underestimated, leading to poor model performance (EF -0.58; Fig. 5).

3.3 Model behavior when aggregate formation was removed

Removing the aggregate protection from the calibrated SAMM model to derive SAMMnoAgg showed that the model assigned
265 a high importance to aggregate protection for the process of SOC stabilization. Without aggregate protection, the simulated SOC of all treatments was reduced to approximately half compared to the measured values (Fig. 7; Table 5b). As a result, all litter addition treatments had approximately the same amount of simulated SOC (excluding litter) in SAMMnoAgg, despite their difference in C/N ratios, lignins, and polyphenols (Fig. 7). Hence, removing aggregate protection led to a significantly reduced and now negative modeling efficiency (-3.68) for SOC (Table 5). In addition, the simulation of microbial nitrogen
270 was negatively affected by the removal of aggregate protection. Due to the absence of aggregate protection of LAB_C and STR_C (i.e. POM), simulated microbial growth became too high after litter addition. However, it still had a positive modeling efficiency (reduction of EF to 0.13 from 0.24, initially) and the temporal trend of the strongest microbial growth occurring
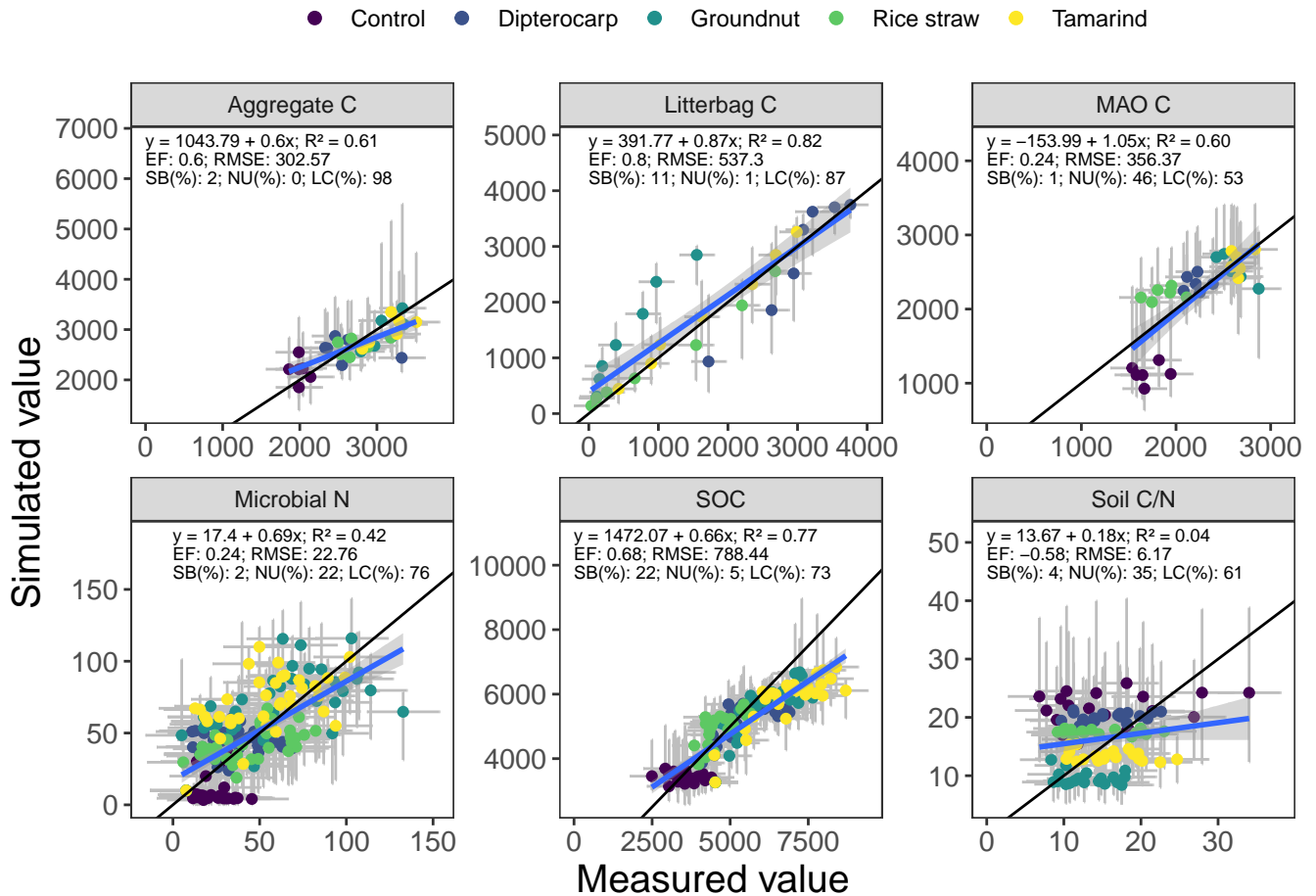
14

Figure 5. Simulated versus measured values of aggregate carbon, litter carbon, mineral-associated organic carbon (MAOC), microbial biomass nitrogen, soil organic carbon (SOC) and soil C/N ratio. The grey bars indicate the 95% credibility interval. The black line marks the 1 to 1 line, the blue line the regression of simulated on measured values.
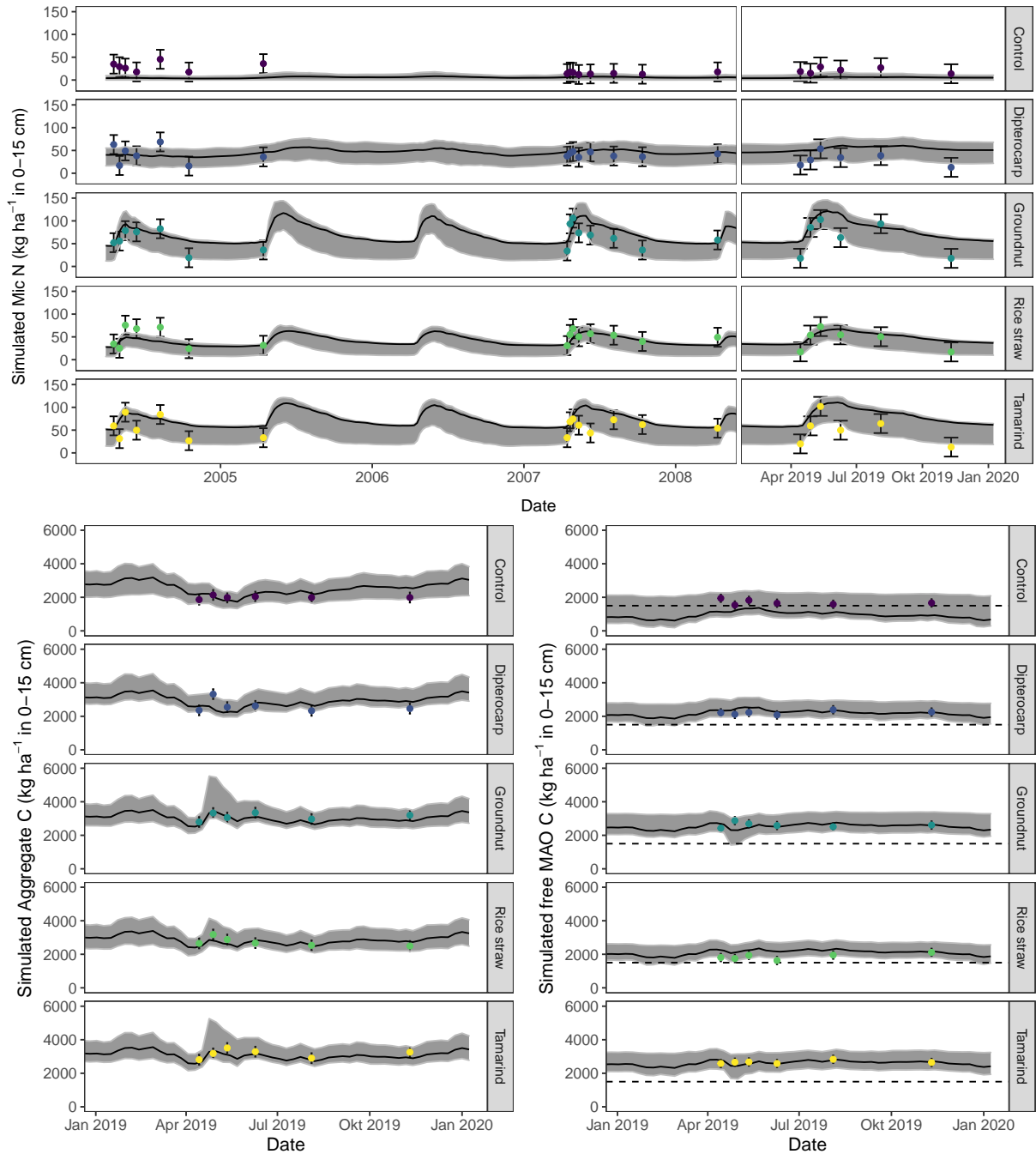
Figure 6. Simulation of microbial nitrogen (MIC_N) in 2005, 2008 and 2019 (top) and of aggregate protected C (Agg_C; bottom left) and free mineral-associated C (MAO_C; bottom right) of different residues in 2019. Dots with error bars indicate the mean and 95% credibility intervals of measured values. The black line and grey band indicate the best simulation and the 95% credibility intervals of the Bayesian calibrations' posterior, respectively. The dashed line indicates the mean free MAO_C in the control in 2019
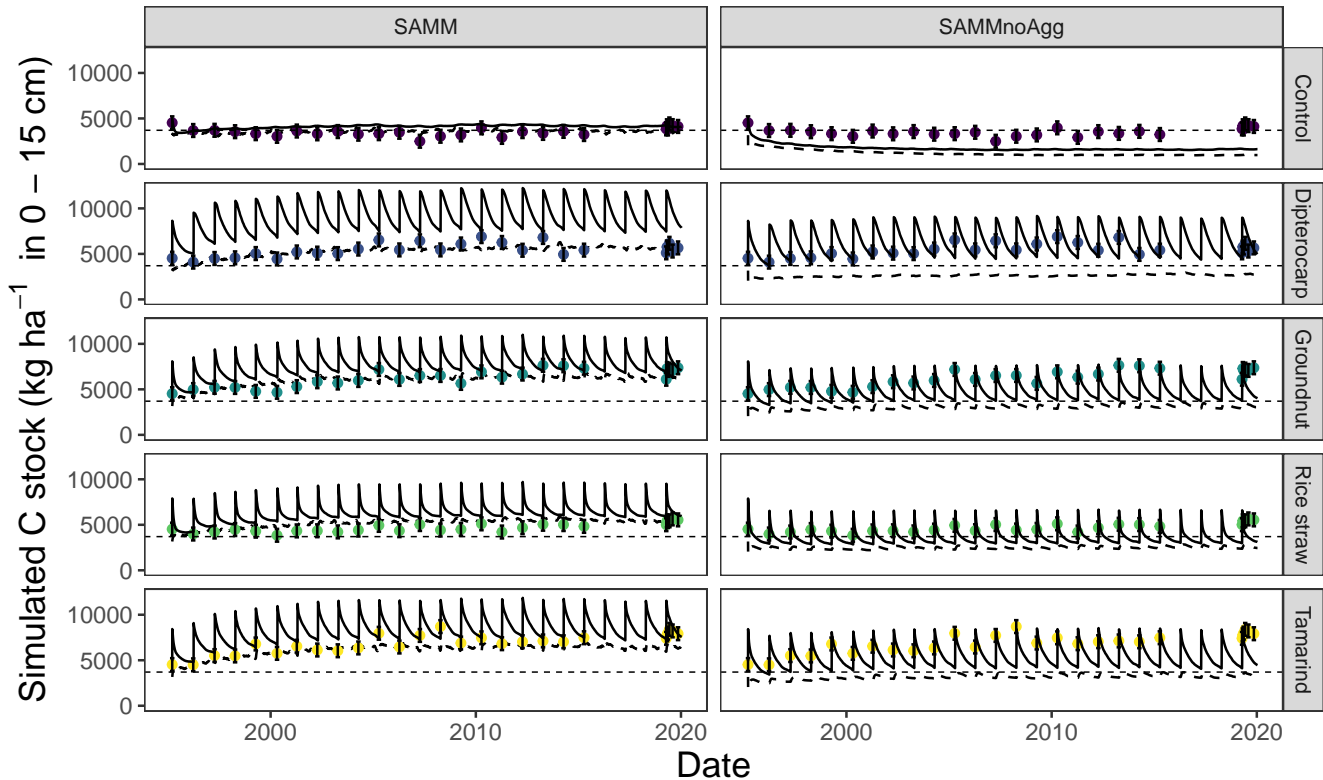
Figure 7. Results for the simulation of carbon stocks with the model version including aggregates (SAMM, left) and when aggregate protection is removed without recalibration (SAMMnoAgg, right). The solid line indicates all carbon including litter, the dynamic dashed line indicates the combined soil carbon stocks stored in MAO_C, Agg_C and MIC_C. The horizontal dashed thin line indicates the mean measured SOC in the control. Dots with error bars indicate the mean and 95% credibility intervals of measured values (excluding litter).

after litter addition was still represented (simulation not shown). In contrast, removing aggregate protection had little effect on the simulation of litterbag carbon (EF was 0.79) and the increase in model error was minor because litterbag carbon is not

275   protected by aggregates. Overall, the dipterocarp treatment was simulated to have the highest carbon storage of litter and SOC combined without aggregate protection. This was mainly because not all dipterocarp litter decomposed within one year.

3.4 Comparison of SAMM separately calibrated with and without the aggregate protection mechanism

When the SAMM model without aggregate formation (SAMMnoAgg) was recalibrated, the poor model performance was largely resolved (Table 5c). For example, the model performance for SOC were the same for the two models (EF of 0.68).

280   However, some notable difference between SAMM and recalibrated SAMMnoAgg remained for the microbial nitrogen and litter carbon. Their dynamics were simulated slightly worse in recalibrated SAMMnoAgg compared to SAMM (EF of 0.80 versus 0.75 for litterbag C and EF of 0.24 versus 0.18 for microbial nitrogen; Table 5c). Consequently, the overall model

17

Table 5. Model evaluation statistics of a) the default SAMM model (with aggregate protection), b) the SAMM model without aggregate protection (SAMMnoAgg), and c) the recalibrated SAMM model without aggregate protection (AMMnoAgg). The RMSE and the width 95% credibility intervals (w95% CI) are in kg ha^{-1}. Evaluation statistics are from the Bayesian calibration. Abbreviations: EF, Nash-Sutcliffe modelling efficiency; (R)MSE, (root) mean squared error; LC, lack of correlation; NU, nonunity slope; SB, squared bias; AIC, Akaike information criterion. Data rows in brackets were not used in the calculation of the overall model AIC.

	dataset	EF	RMSE	R^2	LC	NU	SB	MSE	AIC	% in 95%CI	w95% CI[a]	
	a) Default SAMM model								**5351[b]**			
	Litterbag C	0.80	537.3	0.82	87	1	11	288685	869	64	926	
	Microbial N	0.24	22.8	0.42	76	22	2	518	2041	53	36	
	SOC	0.68	788.4	0.77	73	5	22	621636	2534	62	1381	
(	Aggregate C	0.60	302.6	0.61	98	0	2	91548	521	93	1265	)
(	Free MAO C	0.24	356.4	0.60	53	46	1	126997	664	93	1188	)
(	Soil C/N[c]	-0.58	6.2	0.04	61	35	4	38	1201	61	12	)
	b) Removing aggregate protection/formation (SAMMnoAgg)								**11799[b]**			
	Litterbag C	0.79	540.4	0.81	89	1	10	291993	896			
	Microbial N	0.13	24.4	0.38	70	22	8	594	2183			
	SOC	-3.68	2922.3	0.62	8	2	90	8539715	8855			
	c) Recalibrated SAMMnoAgg								**5554[b]**			
	Litterbag C	0.75	600.4	0.77	89	3	8	360447	993	64	953	
	Microbial N	0.18	23.7	0.39	75	25	0	563	2112	51	38	
	SOC	0.68	792.3	0.75	77	19	4	627769	2540	55	1409	
(	Soil C/N[c]	-133262	1791	0.00	0	99	1	3211117	Inf	65	41	)

[a]95% witdh of the credibility interval from the Bayesian calibration posterior; [b]Overall model AIC. For comparability of model versions this was computed without Aggregate and MAO C and soil C/N. [c]Not used in calibration.

AIC, considering, for comparability, only litterbag carbon, microbial nitrogen, and SOC, was slightly lower for SAMM versus recalibrated SAMMnoAgg (5351 versus 5554).

285   When comparing the posterior distributions of both model versions, it became evident that the recalibration of SAMMnoAgg counteracted the loss of aggregate protection by lowering the turnover turnover of MAOM by almost an order of magnitude (about 85%; Fig. A1). This indicates that the representation of aggregate protection on SOC was changed from explicit to implicit. Also, the recalibrated SAMMnoAgg version had a lower half saturation constant for direct adsorption of $LMW_{C\&N}$ to MAOM in tendency, allowing for a faster direct adsorption (Table 4). However, the removal of aggregate protection did

290   not affect most other model parameters, which were similar in their posterior distributions between SAMM and recalibrated SAMMnoAgg. Interestingly, the 95% posterior credibility intervals were smaller for SAMM than for recalibrated SAMMnoAgg and at the same time covered a higher proportion of measurements of microbial nitrogen and SOC, indicating that they were more accurate for the aggregate version of SAMM.

3.5 Analysis of model parameter behavior

295 In both calibrated model versions, SAMM and SAMMnoAgg showed a clear distinction between the turnover of different carbon pools (Fig. A1). The highest likelihood turnover rates of MAOM, structural and metabolic litter differed by a factor of five to ten (e.g., around 0.0004, 0.002 and 0.02 for SAMM, respectively; Table 4). The breakdown of aggregates, with around 3% per day, as well as the physicochemical aggregate formation, equivalent to a MIC_C growth of 31 kg ha^{-1} per day, were high in SAMM. This indicated a highly dynamic aggerregate fraction and a high importance assigned to physicochemical

300 aggregate formation. At the same time, few strong parameter correlations of r > 0.4 were present in the posterior parameters set for the SAMM (Fig. A2) and the parameter correlations in the recalibrated SAMMnoAgg were of similar magnitude (Fig. A3). First, structural litter turnover and structural protection capacity for labile litter were correlated (r = 0.48). Then, there was a negative correlation between the aggregate protection of POM by microbial growth and the rate of formation of physicochemical aggregates (r = -0.43). Furthermore, the adsorption speed of LMW_C to MAO_C and the turnover of MAOM

305 were correlated (r = 0.40). Finally, the turnover of MAOM was correlated with microbial death (r = 0.42).

4 Discussion

4.1 SAMM as a state-of-the-art soil model with measurable pools

With SAMM, we present a state-of-the-art microbe-driven coupled C/N model that is suitable for field-scale application. It simulates the effect of residue stoichiometry on microbial CUE (Sinsabaugh et al., 2016) and the role of microbial growth in

310 aggregate formation (Laub et al., 2022; Bucka et al., 2021). It contains measurable pools, is well able to simulate aggregate formation resulting from microbial growth, maintains carbon and nitrogen identity (Wang et al., 2022) within the aggregates, and can easily be converted into a lower complexity model without aggregates (i.e., SAMMnoAgg). The model evaluation statistics (Table 5) showed that SAMM, with its representation of carbon and nitrogen in measurable pools (including litter as measurable structural and metabolic pools), is capable of capturing the relevant processes in a long-term experiment of litter

315 addition in a tropical sandy soil and handling the complexity of microbial driven aggregate formation for different chemical compositions of litter. As demonstrated, SAMM captures the differences between treatments, the temporal development of microbial biomass, and the connection between microbial growth and aggregate formation. To our knowledge, apart from an early attempt to model in-situ aggregate stability without considering aggregate stored carbon (Abiven et al., 2008), SAMM is the first model to demonstrate this capability in a field experiment with different litter qualities.

320 The fact that the parameter correlations were low (maximum r = 0.48) compared to calibration exercises with established models such as DayCent (Necpálová et al., 2015, showed parameter correlations between turnover times of different pools of up to r = 0.9), Daisy (Laub et al., 2020, had parameter correlations between turnover of fast and slow pools of up to r = 0.8) or ICBM (Ahrens et al., 2014, had correlations between pools up to r = 0.7), gives some indication that the structure of the SAMM model with measurable pools has a clear advantage compared to models with theory-based conceptual pools. It could,

325 however, also be due to the superiority of Michaelis Menten to first-order kinetics. Furthermore, the fact that all pools can be

measured facilitates calibration, as was recently shown on a global scale with Millennial compared to Century (Abramoff et al., 2022). However, the data needed to constrain models with measurable pools at the global scale may not be readily available. For example, we are not aware of other field experiments that include different litter types and follow microbial biomass, SOC, and aggregate carbon simultaneously over time. Therefore, this version of SAMM was tested only at one site, and it remains 330 to be evaluated for larger spatial scales and with a range of experiments with different quality organic amendments. It is likely that across a range of sites, SAMM model performance will be lower and that the calibration to the single site of this study resulted in an overfitting of some parameters.

We posit that maintaining the carbon identity inside aggregates represents the next logical step for aggregate models, but we are aware of the fact that the marginally better performance of SAMM vs. recalibrated SAMMnoAgg only provides ini- 335 tial evidence. Hence, we invite others to test the concept against further data sets with SAMM or with their own model. By maintaining the carbon identity, aggregate models can help answer important scientific questions, such as how important stabilization of carbon in aggregates is for the global carbon cycle. As shown by the deactivation of aggregates in SAMMnoAgg, SAMM can also provide novel insights into the relative importance of different processes, such as the importance of aggregate protection for carbon stabilization versus protection by attachment to minerals (Angst et al., 2021). In this calibration exercise, 340 the model estimate was that only half of the carbon is protected as MAOC and that about half of the carbon is protected inside aggregates (Fig 7). However, because we had no measurements of POM versus MAOM in the aggregates, we cannot evaluate this by measurements, and it is based on the assumption of complete protection of POM and MAOM inside the aggregates. Another interesting process insight was that the calibration of SAMM assigned a similar importance to physicochemical aggregate formation and microbial aggregate formation and that both processes probably happen in parallel, especially in tropical 345 soils, as tested here. However, it is clear that our data did not provide enough information to clearly distinguish between both processes, which can be seen by the wide posterior credibility intervals of physicochemical aggregate formation. Despite this, the fact that SAMM could simulate the observed increase in aggregate C in the dry season towards the end of 2019 (Fig 6) indicates that this process needs to be included.

4.2 Is aggregate protection necessary to better simulate microbial and SOC dynamics?

350 It has been postulated that because a substantial portion of soil carbon is located within soil aggregates, soil aggregation needs to be included in models to accurately capture reality (Segoli et al., 2013; Abramoff et al., 2018). In this paper we followed this hypothesis and explicitly tested it by comparing the performance of SAMM with and without aggregate formation in simulating litter carbon, microbial nitrogen, and SOC across the different treatments (Table 5). Since clear connections between microbial growth and aggregate formation have been demonstrated (Laub et al., 2022; Bucka et al., 2021; Bossuyt et al., 2001; Denef 355 et al., 2001), including aggregate formation in SAMM is a more realistic process representation. In alignment with our second hypothesis, removing the soil aggregate formation did, even after recalibration of SAMMnoAgg, reduce model performance of the non-aggregated pools, albeit not strongly. This suggests that simulation of aggregate formation and disruption can be useful to understand the overall dynamics of SOC, but that SAMMnoAgg was able to artificially compensate for the missing aggregate protection mechanism (which, as shown by crushed aggregates incubation, e.g., Kpemoua et al., 2022; Puttaso et al.,

360 2011; Six et al., 2002, clearly exists) by reducing turnover of MAOM. What also speaks for this effect are the smaller posterior credibility intervals of SOC, microbial nitrogen, and litter carbon of the aggregate version of SAMM compared to recalibrated SAMMnoAgg (Table 5) and that they still covered a higher percentage of measured values.

The fact that the recalibrated SAMMnoAgg model still seems to implicitly account for the aggregate protection of SOC by reducing the turnover of MAOM (Fig. A1) could suggest that aggregate formation does not need to be included in models

365 to accurately capture differences in SOC formation at large scales. Despite being a better process representation, limited data availability of aggregate- and microbial dynamics may make a non-aggregate model more feasible. However, for a mechanistic understanding, i.e., using the model as a research tool to test hypotheses, it is arguably better to include aggregate formation and carbon protection in aggregates. In contrast, simulating aggregate protection may not be necessary to assess the carbon sequestration potential of different management strategies. On the one hand, many processes that are relevant for soil formation

370 and SOC stabilization and occur inside aggregates, may be irrelevant at the field scale (Yudina and Kuzyakov, 2019) if they are implicitly included by adjusting other model parameters. On the other hand, we only had data to test SAMM with one long-term experiment in a single soil type. Model parsimony and equifinality often depend on how much data is available (Marschmann et al., 2019). Hence, it is possible that across sites, the interaction of factors such as differences in texture, litter composition, and different climates on SOC protection may be best represented by a model that includes the mechanism of

375 aggregate protection. For example, the better model performance of Millenial compared to Century only became evident when looking at the global distribution of soil carbon (i.e., only at high latitudes is Millenial better; Abramoff et al., 2022). Clearly, a range of field experiments that measured the temporal dynamics of aggregates together with microbial biomass and SOC would be needed to better test and hence understand the relevance of aggregate formation to simulate SOC dynamics across scales.

380 ## 4.3 Potential limitations and open questions

An interesting observation is that the model assumes a rather high amount of daily carbon input through roots (about 3 kg C ha^{-1} day^{-1} for both SAMM and SAMMnoAgg) in addition to the litter that is added annually through the treatment. However, this additional material is expected to have a rather high C/N ratio. The parameter of daily carbon input was included for two reasons: 1) we observed weed growth in the plots, despite regular weeding, and hence assuming no additional inputs did not

385 seem reasonable, and 2) model runs with carbon inputs only from litter addition could not maintain any microbial activity in the control, further corroborating the validity for these inputs (simulations not shown). The fact that the calibration assumed rather high root inputs is potentially due to the absence of more complex microbial traits in SAMM, such as dormancy, which some other models include (Wang et al., 2015; Blagodatsky and Richter, 1998). In fact, the estimation of microbial biomass via chloroform fumigation extraction does not separate between dormant and active microbes. While Wang et al. (2015) suggested

390 that a model that includes dormancy can better represent the total magnitude of microbial biomass, an important concept of SAMM was the measurability of all pools and the inclusion of dormancy would thus need data on dormancy, which was not available in this trial. Ideally, only the non-dormant microbes should be considered in the microbial activity factor (a_{MIC}). Since $K_{M_{MIC}}$, which determines a_{MIC}, is a calibrated parameter, this discrepancy does not drastically alter model behavior. However,

it means that the microbial activity factor of SAMM cannot be directly compared to measurements of microbial activity, and it implicitly assumes that the fraction of dormant microbes is constant. Since the water and temperature rate modifiers indirectly account for differences in microbial activity between optimal and poor conditions, the use of chloroform fumigation extraction data is most likely, in the absence of data on dormancy, the best way to represent a single microbial biomass pool while maintaining structural identity.

Furthermore, CUE is only a function of litter C/N and not of the microbial community. An earlier study showed that the different treatments led to different microbial communities (Kamolmanit et al., 2013), and communities of minimal inputs usually become more efficient at recycling carbon and nitrogen (Dijkstra et al., 2022). The lower C/N ratio of daily root carbon inputs in SAMMnoAgg compared to SAMM in that regard could be interpreted as aggregate formation within a model that helps simulate microbial biomass patterns. In fact, aggregate formation, linked to both microbial growth and physicochemical formation, was very fast. Additionally, turnover rates were high (almost as fast as metabolic litter decomposition). This is in alignment with a recent model of aggregation on the micro scale (Zech et al., 2022). Yet, it is difficult to distinguish between the different pathways of aggregate formation. Finally, the question is to what extent POM and MAOM are effectively protected inside aggregates. In this version of SAMM, we simulated the most extreme case of complete protection of carbon inside aggregates, which in future versions should most likely be replaced by a decomposition reduction factor because we know that aggregates do not completely protect carbon. Yet, it will be very difficult to measure carbon turnover inside aggregates and hence to constrain such a reduction factor. Finally, the next logical step would be to include multiple soil layers in SAMM, provided a suitable water leaching function is included. The $LMW_{C/N}$ leaching to deeper soil layers, feeding aggregate formation there should, in theory, help to explain SOC depth gradients.

5 Conclusions

We presented and evaluated the SAMM model, a state-of-the-art soil organic matter research model with measurable pools that can simulate the formation and turnover of aggregates under different organic amendment treatments. Overall, good model evaluation statistics (EF 0.2 to 0.8, depending on observation type) and low parameter correlations (r < 0.48) suggested that the current structure of SAMM is valuable, clearly identifiable in calibration and hence parsimonious. The results suggested that aggregate protection plays a crucial role for SOC stabilization, i.e., in the model simulations about 50% of soil carbon was protected in aggregates, even in the sandy soil of the studied long-term experiment. While for basic research, aggregate formation should be included into models, our results indicate that with model recalibration, the absence of aggregate protection in SOM models is partly compensated by reducing turnover of the MAOM pool. Hence, if the sole goal is to represent SOM, microbial nitrogen, and litter carbon well, aggregate formation may be omitted in SOM models, especially if insufficient data on aggregates exists. However, it is possible that this compensation within our study was only possible because the data originated from a single site. For further evidence, studies would be needed in a variety of soils and climates, which calls for more long-term studies to include repeated measurements of aggregate and microbe dynamics.

22

Appendix A: Appendix

A1   Detailed description of the SAMM model pools

A1.1   Structural litter pool - STR_C

To make the structural litter pool (STR_C) fully measurable, it consists of lignin and polyphenols, the parts of litter which stabilize the cell wall and are processed by microbes with a low CUE. STR_C is assumed to have a carbon content of 65%, representing a lignin-typical C/H/O ratio of 20/23/7 (Gargulak et al., 2015). Through this definition, the structural litter pool is measurable as acid detergent lignin (Van Soest and Wine, 1968) and polyphenols (Anderson and Ingram, 1993), and it does not contain nitrogen.

A1.2   Metabolic litter pool – LAB_C and LAB_N

The metabolic litter pool contains all parts of the litter which are not part of STR_C. This includes cellulose, hemicellulose, intracellular carbon, and nitrogen. Because plant cell walls are a mixture of structural components with celluloses and hemi-celluloses (Alberts et al., 2002), there needs to be a distinction between the non-lignin components of the cell wall and the easily available cell interior. While others have solved this by creating three litter pools, containing the soluble part, the non-lignin structural part and the lignin part (Campbell et al., 2016), we wanted to be parsimonious and have only two litter pools. We therefore linked the decomposition speed of the non-lignin cell wall components to the decomposition speed of lignin by adding a simulated protection capacity of the structural litter pool on the metabolic litter pool. This mimics that the parts of the cellulose, hemicellulose and lignin of the cell wall are tightly interwoven (Alberts et al., 2002). The amount of protected metabolic carbon ($ProtLAB_{C\&N}$) is not a real pool but a linear function of carbon in the structural pool (fixed ratio). This approach implicitly assumes that non-lignin and lignin cell wall components decompose together and that the decomposition speed of the lignin components is the rate-limiting factor. All components that are not protected by STR_C are considered to be easily available for microbial uptake and, due to the lower cost of depolymerization, microbes usually process them with a higher CUE.

A1.3   Low molecular weight carbon and nitrogen pools - LMW_C and LMW_N

The low molecular weight pool contains depolymerized carbon and nitrogen which easily enters the soil solution. All de-composed plant and microbial residues, as well as MAOM, end up in this pool. The pool of $LMW_{C\&N}$ can be measured by extraction using a K_2SO_4 solution. Microbes, similar to other established models, such as MEND (Wang et al., 2013) and Millenial (Abramoff et al., 2018), can only consume carbon and nitrogen in the $LMW_{C\&N}$ pool. When consumed by microbes,

LMW_C is subject to a dynamic CUE. This dynamic CUE is a function of the C/N ratio of $LMW_{C\&N}$, thus accounting for a C/N-dependent growth respiration and spilling (Sinsabaugh et al., 2013). We used the linear function of C/N dependent CUE (Fig. A6) based on Campbell et al. (2016, equation 16B), which they based on Sinsabaugh et al. (2013). Additionally, the $LMW_{C\&N}$ pool is the only pool that can be leached. Finally, direct adsorption of LMW_C and LMW_N to particles from the silt and clay fraction is possible. This was simulated using a Langmuir-type relationship, as in Wang et al. (2013), with values for this relationship estimated by Abramoff et al. (2022).

A1.4   Microbial pools - MIC_C and MIC_N

The $MIC_{C\&N}$ pool comprises the living soil microbial biomass that actively influences the decomposition of all other pools. $MIC_{C\&N}$ can be measured using various techniques, such as substrate-induced respiration (Kandeler et al., 1999), or the more common chloroform fumigation extraction (Vance et al., 1987), but all of these are subject to considerable uncertainty. In SAMM, the $MIC_{C\&N}$ pool actively contributes to the decomposition of other pools through a microbial activity factor (a_{MIC}). Because the uptake of LMW_C and LMW_N by microbes only depends on the availability and on a_{MIC}, the C/N ratio of microbes is not fixed. We included indirect limits to microbial C/N through a C/N-dependent CUE and a direct limit through nitrogen immobilization if microbial C/N surpasses an upper boundary and a spilling of nitrogen occurs for very low C/N ratios at a lower boundary. If the C/N ratio of microbes becomes smaller than a minimum C/N, the excess nitrogen is released by the microbes to avoid unrealistically low C/N ratios of the microbes (maximally half of the excess nitrogen per day). Both maximum and minimum microbial C/N are calibrated parameters. The microbial pool is subject to maintenance respiration and microbial death. The carbon and nitrogen of dead microbes are divided between the $LMW_{C\&N}$ and the mineral-associated pool, representing the soluble cell constituents entering $LMW_{C\&N}$ and cell wall structures, which are assumed to be attached directly to the minerals (Krause et al., 2019).

A1.5   Mineral-associated organic carbon and nitrogen pools – MAO_C and MAO_N

This pool consists of all carbon and nitrogen which is attached to silt and clay. It has long been suggested that this is a form of carbon and nitrogen with slower average turnover than total SOM (Christensen, 2001) with a residence time of decades to millenia (Kögel-Knabner et al., 2008). There are two ways in which carbon and nitrogen can enter the $MAO_{C\&N}$ pools: first, microbial cell walls that attach to minerals after microbial death and second, the adsorption of $LMW_{C\&N}$. As in many models, we allow for an attachment of SOM to $MAO_{C\&N}$ in the form of microbial residues that is only limited by a partitioning constant as one process. The adsorption of $LMW_{C\&N}$ to $MAO_{C\&N}$, as the other process, follows a Langmuir-type relationship, where the limit is determined by the amount of silt and clay in a soil (Abramoff et al., 2022). The differences between $LMW_{C\&N}$ and $MIC_{C\&N}$ attachment to $MAO_{C\&N}$ follow recent studies that demonstrated that N-rich microbial products preferentially attach to new mineral surfaces (Kopittke et al., 2018, 2020), while the direct sorption of $LMW_{C\&N}$ depends on the amount of fine particles (Georgiou et al., 2022).

A1.6 Aggregate pools – Agg_C and Agg_N

To adhere to the concept of structural carbon identities, the carbon and nitrogen in aggregates does not represent a single pool. Instead, the aggregates consist of the primary constituents STR_C, $LAB_{C\&N}$ and $MAO_{C\&N}$ pools, which inside aggregates are protected from decomposition ($AggSTR_C$, $AggLAB_{C\&N}$ and $AggMAO_{C\&N}$). In alignment with recent studies showing that the presence of microbially-produced binding agents stabilizes aggregates (Bettermann et al., 2021; Crouzet et al., 2019), the rate of aggregate formation in SAMM (amounts of primary constituents entering the aggregate protected pools) is a function of microbial growth. Furthermore, SAMM allows for physicochemical aggregate formation at a constant rate (currently defined as daily microbial growth equivalent). This physicochemical aggregate formation represents all abiotic aggregate formation processes. Hence, SAMM allows for both important processes of aggregate formation; biological and physicochemical (Six et al., 2002). While within the aggregates there is no decomposition, a concept proposed by Luo et al. (2017) as a way to reduce the number of parameters in aggregation models and represent aggregate protection in a parsimonious way. Each carbon identity is transferred back into the pool from which it originated without any loss of matter during aggregate turnover.

A2 Technical implementation of SAMM

The SAMM model was written in the R programming language (R Core Team, 2020), and differential equations were solved using the deSolve package with the rk4 solver (Soetaert et al., 2010). Thus, it can be run at any time step. We used a daily time step with the optimized rk4() solver, after confirming that the results for this were the same as using an ode() solver, which makes time steps infinitely small and has no numerical errors. Simulations of carbon and nitrogen dynamics are performed for the topsoil layer (0-15 cm). While all flows of carbon and nitrogen between pools were simulated within the SAMM model, the soil water status, water leaching, and temperature, needed to drive SAMM, are currently external inputs. Climatic data and soil temperature measurements were available from a station located close to the experiment, and soil water content and leaching of water from the soil was simulated with the HYDRUS 1D model (Šimůnek et al., 2005) based on climatic data and soil texture. Measurements conducted with moisture sensors during 2019 showed that the simulated HYDRUS water content matched the moisture levels and the dynamical pattern of the measured water content (Figure A4). To be able to calibrate SAMM for litter decomposition from a litterbag experiment, we created litterbag carbon and nitrogen pools, which were reinitialized with each yearly litter addition and did not flow into any other pools. They decomposed at the same turnover as the normal STR_C and $LAB_{C\&N}$ litter pools, but could not be protected in aggregates. Note that SOC was defined to correspond all pools combined, excluding the free STR_C and LAB_C pools.

A3 SAMM model equations and additional model graphs

The following section describes the differential equations of the SAMM model that govern the changes of pool sizes (Table 3) over time. Inputs into the system are only in the form of litter (I_{STR_C} and I_{LAB_C}). The flows between pools are displayed as flows ($F_{X_1X_2}$) from the donor pool (X_1) to the receiving pool (X_2) as follows:
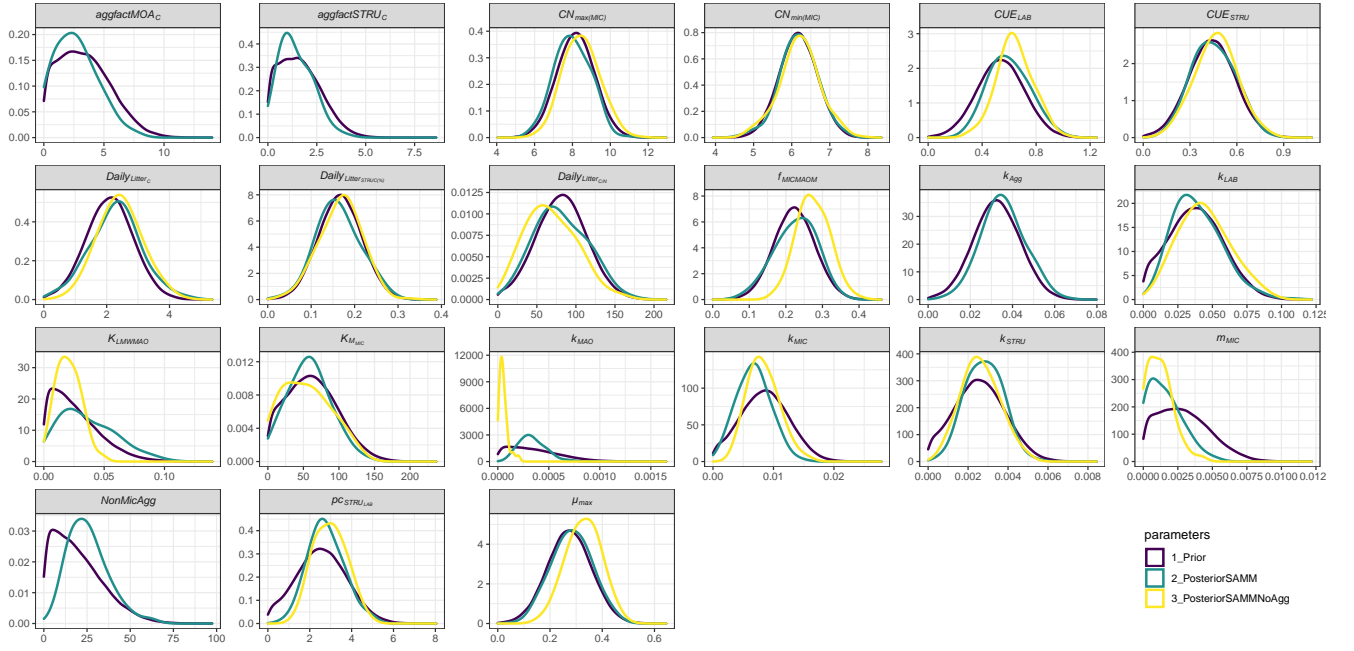
25

Figure A1. Prior and posterior parameter distributions of SAMM and the version without aggregates (SAMMnoAgg) for all model parameters that were calibrated. Priors were the mean of SAMM and SAMMnoAgg from an initial calibration of both model versions with a genetic algorithm. The width of the distribution was manually chosen and based on the range given by the genetic algorithm. Negative values were excluded.

$$\frac{dSTR_C}{dt} = +I_{STR_C} - F_{STR_C LMW_C} - F_{STR_C AggSTR_C} + F_{AggSTR_C STR_C} - F_{STR_C CO_2} \tag{A1}$$

$$\frac{dLAB_C}{dt} = +I_{LAB_C} - F_{LAB_C LMW_C} - F_{LAB_C AggLAB_C} + F_{AggLAB_C LAB_C} - F_{LAB_C CO_2} \tag{A2}$$

520
$$\frac{dLMW_C}{dt} = +F_{STR_C LMW_C} + F_{LAB_C LMW_C} + F_{MIC_C LMW_C} + F_{MAO_C LMW_C} - F_{LMW_C MIC_C} - F_{LMW_C MAO_C} - F_{LMW_C C_{leach}} - F_{LMW_C CO_2} \tag{A3}$$

$$\frac{dMIC_C}{dt} = +F_{LMW_C MIC_C} - F_{MIC_C LMW_C} - F_{MIC_C MAO_C} - F_{MIC_C CO_2} \tag{A4}$$

$$\frac{dMAO_C}{dt} = +F_{MIC_C MAO_C} + F_{LMW_C MAO_C} - F_{MAO_C LMW_C} - F_{MAO_C AggMAO_C} + F_{AggMAO_C MAO_C} \tag{A5}$$

$$\frac{dAggSTR_C}{dt} = +F_{STR_C AggSTR_C} - F_{AggSTR_C STR_C} \tag{A6}$$
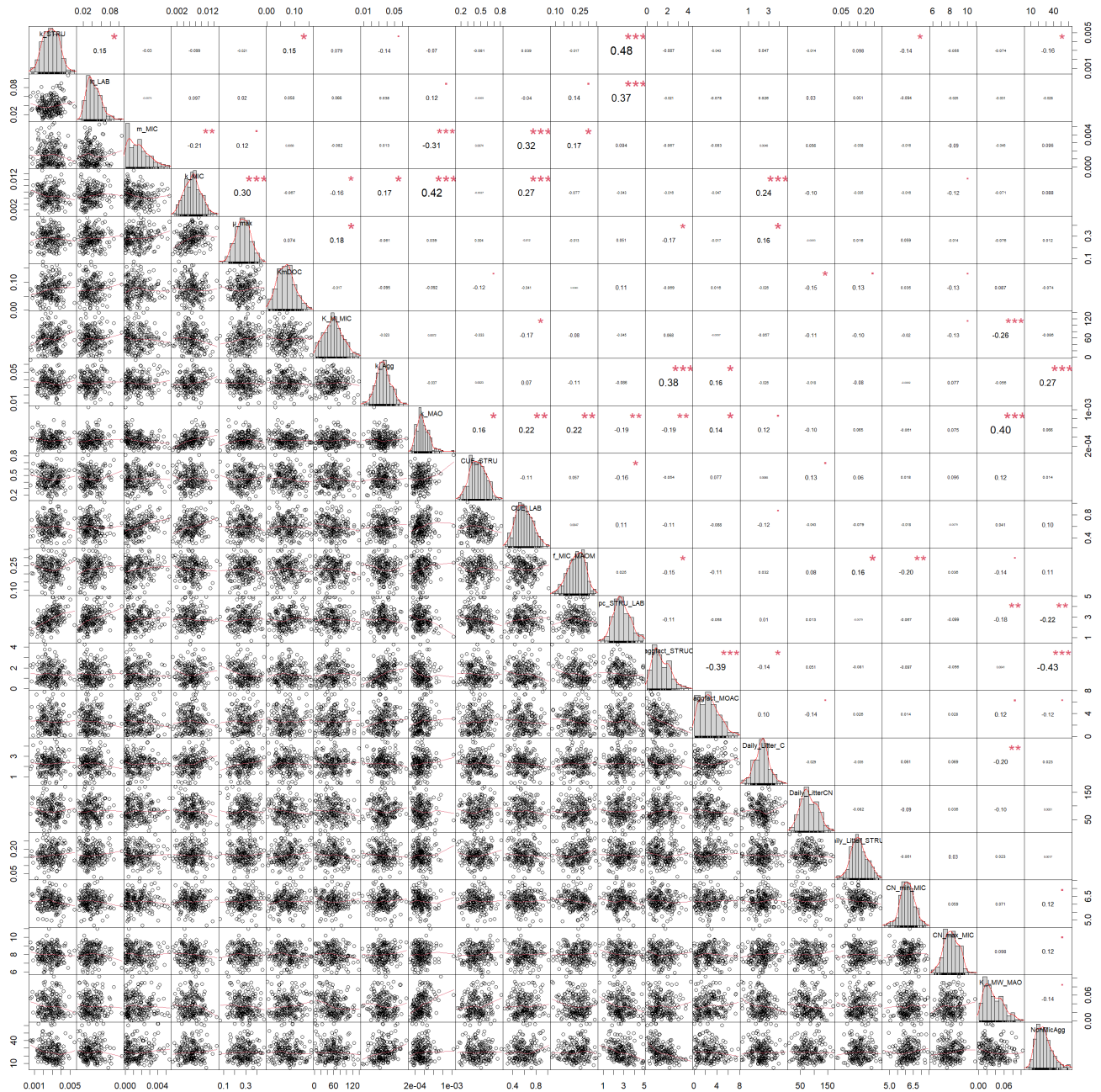
Figure A2. Correlation matrix between all calibrated parameters of the SAMM model. The parameter values are from the posterior distribution of the Bayesian calibration using the SIR method.
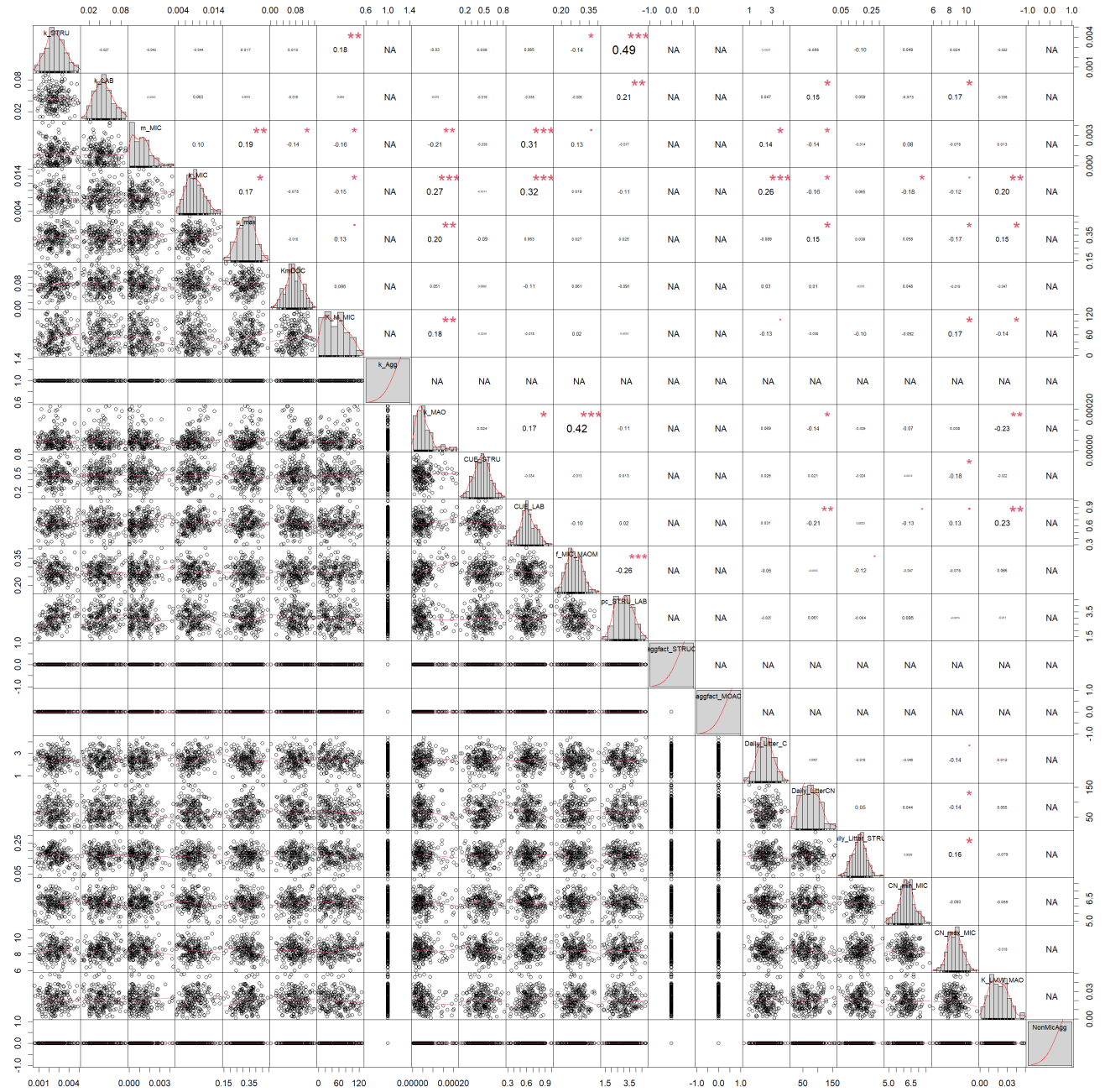
Figure A3. Correlation matrix between all calibrated parameters of the model without aggregates (SAMMnoAgg). The parameter values are from the posterior distribution of the Bayesian calibration using the SIR method. Aggregate related parameters were fixed to deactivate the aggregate formation.
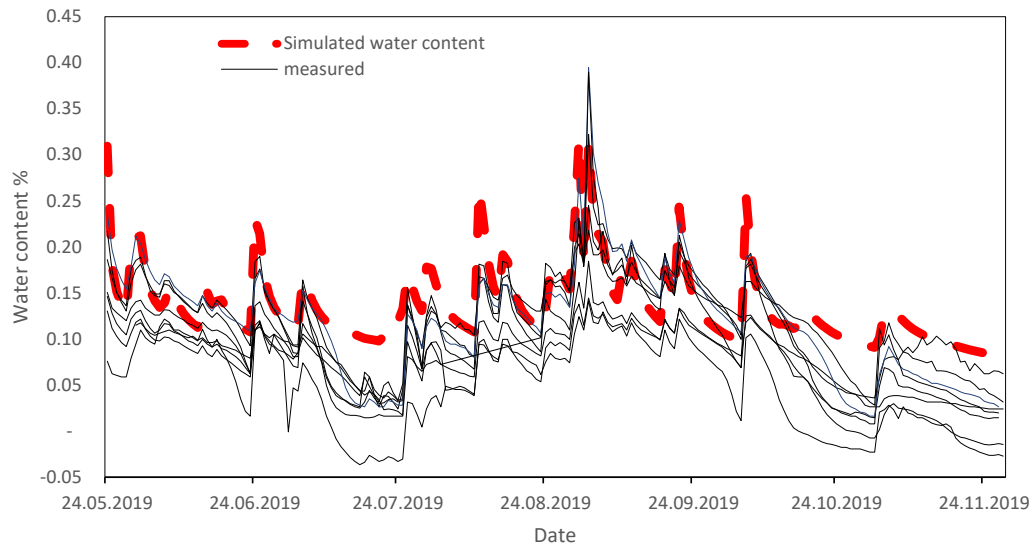
Figure A4. Comparison of measured water contents by moisture sensors (ECH2O EC-5, METER Group, Inc. USA; solid lines) with simulated water content by HYDRUS 1D (red dashed line). Sensors were installed in different plots of the long-term Experiment in Khon Kaen.
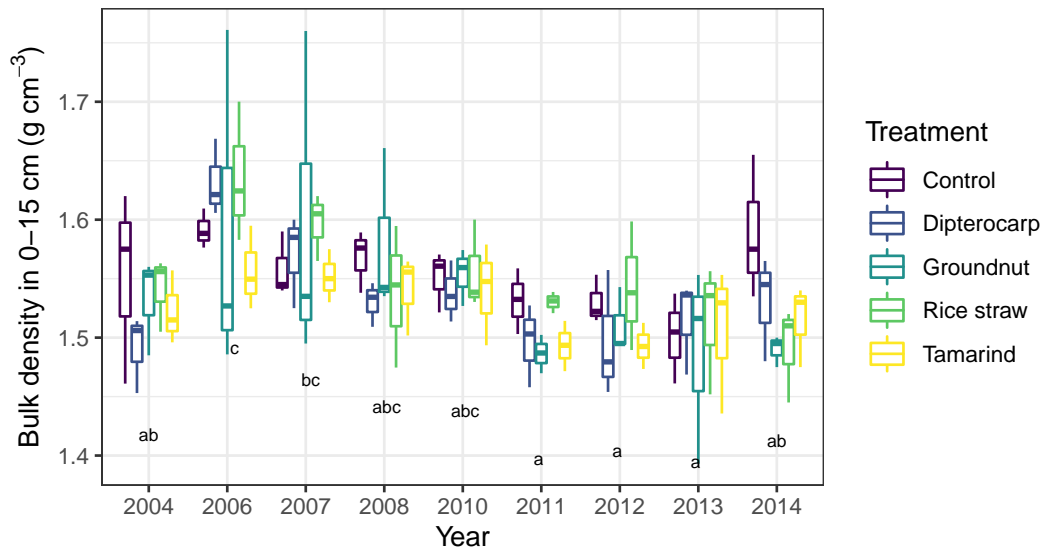
Figure A5. Comparison of measured bulk densities in 0-15 cm in the years with available data. Treatment differences were not significant but a significant effect of year existed. This was however not considered to be any temporal trend but rather an effect arising from different people conducting the sampling. All statistical test conducted with a mixed linear effects model, containing a random intercept per subplot nested in the experimental block.

$$\frac{dAggLAB_C}{dt} = +F_{LAB_C AggLAB_C} - F_{AggLAB_C LAB_C} \tag{A7}$$

525
$$\frac{dAggMAO_C}{dt} = +F_{MAO_C AggMAO_C} - F_{AggMAO_C MAO_C} \tag{A8}$$

Respired (CO_2) and leached (C_{leach}) carbon are permanently lost from the system.

$$\frac{dCO_2}{dt} = +F_{STR_C CO_2} + F_{LAB_C CO_2} + F_{LMW_C CO_2} + F_{MIC_C CO_2} \tag{A9}$$

$$\frac{dC_{leach}}{dt} = +F_{LMW_C C_{leach}} \tag{A10}$$

The flows of carbon between pools, as described above, are computed from the state variables of each pool X_C, the protection
530 capacity for the LAB_C pool ($pLAB$), carbon use efficiencies for each pool (CUE_X) and their standard turnover rates (k_X) or maximum microbial uptake for LMW_C (μ_{max}). Apart from LMW_C, the CUE_X, are not directly measurable, but represent a proxy for depolymerization cost. The decomposition speed of all pools outside aggregates is influenced by a reverse Michaelis-Menten microbial activity factor (a_{MIC}), a temperature (s_t) and a moisture rate modifier (s_w) influences all pools. Partitioning coefficients (f_X) are further used, where one pool feeds into several pools.

535
$$F_{STR_C LMW_C} = STR_C * CUE_{STR} * k_{STR} * a_{MIC} * s_t * s_w \tag{A11}$$

$$F_{STR_C CO_2} = STR_C * (1 - CUE_{STR}) * k_{STR} * a_{MIC} * s_t * s_w \tag{A12}$$

$$F_{LAB_C LMW_C} = LAB_C * (1 - pLAB) * CUE_{LAB} * k_{LAB} * a_{MIC} * s_t * s_w \tag{A13}$$

$$F_{LAB_C CO_2} = LAB_C * (1 - pLAB) * (1 - CUE_{LAB}) * k_{LAB} * a_{MIC} * s_t * s_w \tag{A14}$$

$$F_{LMW_C MIC_C} = LMW_C * CUE_{CN(LMW)} * \mu_{max} * a_{MIC} * s_t * s_w \tag{A15}$$

540
$$F_{LMW_C CO_2} = LMW_C * (1 - CUE_{CN(LMW)}) * \mu_{max} * a_{MIC} * s_t * s_w \tag{A16}$$

The protection and disruption of aggregates is formulated as follows:

$$F_{STR_C AggSTR_C} = min(((F_{LMW_C MIC_C} + NonMicAgg) * aggfact_{STR_C}), STR_C) \tag{A17}$$

$$F_{LAB_C AggLAB_C} = min(F_{STR_C AggSTR_C} * pc_{STR_{LAB}}, LAB_C) \tag{A18}$$

30

$$F_{MAO_C AggMAO_C} = min(((F_{LMW_C MIC_C} + NonMicAgg) * aggfact_{MAO_C}), MAO_C) \tag{A19}$$

$$F_{AggSTR_C STR_C} = AggSTR_C * k_{Agg} * s_t * s_w \tag{A20}$$

$$F_{AggLAB_C LAB_C} = AggLAB_C * k_{Agg} * s_t * s_w \tag{A21}$$

$$F_{AggMAO_C MAO_C} = AggMAO_C * k_{Agg} * s_t * s_w \tag{A22}$$

$$F_{MIC_C CO_2} = MIC_C * m_{mic} * s_t * s_w \tag{A23}$$

$$F_{MIC_C LMW_C} = MIC_C * k_{mic} * (1 - f_{MICMAOM}) * s_t * s_w \tag{A24}$$

$$F_{MIC_C MAO_C} = MIC_C * k_{mic} * f_{MICMAOM} * s_t * s_w \tag{A25}$$

$$F_{MAO_C LMW_C} = MAO_C * k_{MAO} * a_{MIC} * s_t * s_w \tag{A26}$$

Adsorption to MAOC is formulated as follows:

$$F_{LMW_C MAO_C} = LMW_C * K_{LMWMAO} * \frac{MAO_{C_{max}} - MAO_C}{MAO_{C_{max}}} * s_t * s_w \tag{A27}$$

For leaching, which was externally calculated using the HYDRUS 1D model (Šimůnek et al., 2005) it is assumed that $LMW_{C\&N}$ are equally mixed with the soil solution and thus lost at the same rate as leached water.

$$F_{LMW_C C_{leach}} = min(w_{leach} * LMW_C; 0.95 * LMW_C) \tag{A28}$$

The reverse Michaelis-Menten microbial activity factor (a_{MIC}), which influences the decomposition speed of most pools, the ratio of STR_C, $LAB_{C\&N}$ and $MAOC_{C\&N}$ protected in aggregates are calculated as follows:

$$a_{MIC} = max(\frac{MIC_C}{K_{M_{MIC}} + MIC_C}; 0.05) \tag{A29}$$

It was defined as never being lower than 0.05, so that microbes in low organic matter input treatments would not completely die off.

The maximum adsorption capacity of a soil depends on the modeled depth, the bulk density (BD) and the amount of silt and clay particles (SiCl):

$$MAO_{C_{max}} = depth * BD * \%SiCl * c_{SORP} \tag{A30}$$

The temperature (s_t) and a moisture scalar (s_w) and the dynamic CUE were adopted from established models and not subject to further modification (Fig. A6). For the temperature scalar, an exponential equation was chosen as is common in many models (e.g. Daisy; Hansen et al., 1993). In this context it is important to note that different temperature rate modifiers have a different temperature at which they set the temperature scalar to 1. Here 20°C was chosen to be representative for the tropical climates. Many temperate models use a value of 10°C for the scalar (Daisy, RothC), whereas Century and Millenial use a scalar that has a maximum value of 1 at 40°C but only 0.5 at 20°C. This difference in temperature scalar functions needs to be considered, for example, when adopting turnover rates from one model to another. In that case, rates need to be adjusted accordingly (e.g. in the case of SAMM multiplying them by 2 for models that define the scalar to be 1 at 10°C and use an exponential temperature function with a Q_{10} value of 2).

$$s_t = 2^{\left(\frac{t-20}{10}\right)} \tag{A31}$$

$$s_w = min\left((0.6 + 0.4 * \frac{pF}{1.5}); max(1.625 - \frac{pF}{4}; 0); 1\right) \tag{A32}$$

$$CUE_{CN(LMW)} = CUE_{LMW} * min\left(CN(LMW)^{-1} * 13.4; 1\right) \tag{A33}$$

The flow of nitrogen between the different pools is simulated in a a way that is similar to the carbon pools:

$$\frac{dLAB_N}{dt} = +I_{LAB_N} - F_{LAB_N LMW_N} - F_{LAB_N AggLAB_N} + F_{AggLAB_N LAB_N} \tag{A34}$$

$$\frac{dLMW_N}{dt} = +F_{LAB_N LMW_N} + F_{MIC_N LMW_N} + F_{MAO_N LMW_N} - F_{LMW_N MIC_N} - F_{LMW_N MAO_N} - F_{LMW_N N_{leach}} - IM_{MIC_N} + OS_{MIC_N} \tag{A35}$$

$$\frac{dMIC_N}{dt} = +F_{LMW_N MIC_N} - F_{MIC_N LMW_N} - F_{MIC_N MAO_N} + IM_{MIC_N} - OS_{MIC_N} \tag{A36}$$

$$\frac{dMAO_N}{dt} = +F_{MIC_N MAO_N} + F_{LMWC_N MAO_N} - F_{MAO_N LMW_N} - F_{MAO_N AggMAO_N} + F_{AggMAO_N MAO_N} \tag{A37}$$

$$\frac{dAggLAB_N}{dt} = +F_{LAB_C AggLAB_N} - F_{AggLAB_C LAB_N} \tag{A38}$$

$$\frac{dAggMAO_N}{dt} = +F_{MAO_C AggMAO_N} - F_{AggMAO_C MAO_N} \tag{A39}$$

$$\frac{dN_{leach}}{dt} = +F_{LMW_N N_{leach}} \tag{A40}$$

To calculate the flows of nitrogen, the same scalars, ratios of protected STR_C, $LAB_{C\&N}$ and $MAOC_{C\&N}$ in aggregates, and turnover rates are used. Additionally, the microbes can immobilize nitrogen (IM_{MIC_N}) from LMW_N, if their C/N ratio gets too wide, or spillover nitrogen to the DON pool (OS_{MIC_N}), if their C/N ratio gets too narrow:
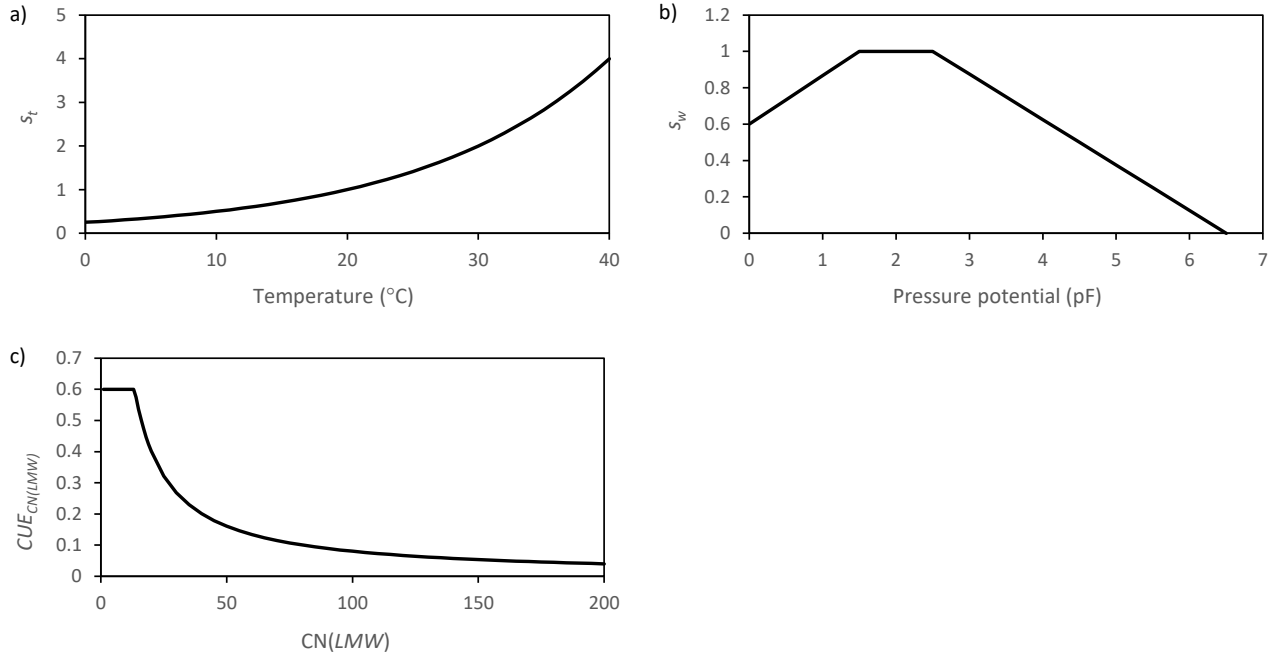
Figure A6. Graphic representation of the scalar functions which are applied in SAMM to represent the effect of a) temperature b) moisture. Additionally the function that represents c) the dynamic *CUE* based on the C/N ratio of $LMW_{C\&N}$ is displayed.

$$F_{LAB_N LMW_N} = LAB_N * (1 - pLAB) * k_{LAB} * a_{MIC} * s_t * s_w \tag{A41}$$

$$F_{LMW_N MIC_N} = LMW_N * \mu_{max} * a_{MIC} * s_t * s_w + IM_{MIC_N} - OS_{MIC_N} \tag{A42}$$

$$F_{MIC_N LMW_N} = MIC_N * k_{mic} * (1 - f_{MICMAOM}) * s_t * s_w - IM_{MIC_N} + OS_{MIC_N} \tag{A43}$$

$$F_{MIC_N MAO_N} = MIC_N * k_{mic} * f_{MICMAOM} * s_t * s_w \tag{A44}$$

$$F_{MAO_N LMW_N} = MAO_N * k_{MAO} * a_{MIC} * s_t * s_w \tag{A45}$$

$$F_{LMW_N MAO_N} = F_{LMW_C MAO_C} * \frac{LMW_N}{LMW_C} \tag{A46}$$

$$F_{LAB_N AggLAB_N} = F_{LAB_C AggLAB_C} * \frac{LAB_N}{LAB_C} \tag{A47}$$

$$F_{MAO_N AggMAO_N} = F_{MAO_C AggMAO_C} * \frac{MAO_N}{MAO_C} \tag{A48}$$

$$F_{AggLAB_N LAB_N} = AggLAB_N * k_{Agg} * s_t * s_w \tag{A49}$$

$$F_{AggMAO_N MAO_N} = AggMAO_N * k_{Agg} * s_t * s_w \tag{A50}$$

600 $$F_{LMW_N N_{leach}} = min(w_{leach} * LMW_N; 0.95 * LMW_N) \tag{A51}$$

$$IM_{MIC_N} = if\left(\frac{MIC_C}{MIC_N} > CN_{max(MIC)}\right)\left[min\left(\frac{MIC_C}{CN_{max(MIC)}} - MIC_N; \frac{1}{2}LMW_N\right); 0\right] \tag{A52}$$

$$OS_{MIC_N} = if\left(\frac{MIC_C}{MIC_N} < CN_{min(MIC)}\right)\left[0.5\left(MIC_N - \frac{MIC_C}{CN_{min(MIC)}}\right); 0\right] \tag{A53}$$

References

Abiven, S., Menasseri, S., Angers, D. A., and Leterme, P.: A Model to Predict Soil Aggregate Stability Dynamics following Organic Residue Incorporation under Field Conditions, Soil Science Society of America Journal, 72, 119–125, https://doi.org/10.2136/sssaj2006.0018, _eprint: https://onlinelibrary.wiley.com/doi/pdf/10.2136/sssaj2006.0018, 2008.

Abramoff, R., Xu, X., Hartman, M., O'Brien, S., Feng, W., Davidson, E., Finzi, A., Moorhead, D., Schimel, J., Torn, M., and Mayes, M. A.: The Millennial model: in search of measurable pools and transformations for modeling soil carbon in the new century, Biogeochemistry, 137, 51–71, https://doi.org/10.1007/s10533-017-0409-7, 2018.

Abramoff, R. Z., Guenet, B., Zhang, H., Georgiou, K., Xu, X., Viscarra Rossel, R. A., Yuan, W., and Ciais, P.: Improved global-scale predictions of soil carbon stocks with Millennial Version 2, Soil Biology and Biochemistry, p. 108466, https://doi.org/10.1016/j.soilbio.2021.108466, 2022.

Ahrens, B., Reichstein, M., Borken, W., Muhr, J., Trumbore, S. E., and Wutzler, T.: Bayesian calibration of a soil organic carbon model using Δ14C measurements of soil organic carbon and heterotrophic respiration as joint constraints, Biogeosciences, 11, 2147–2168, https://doi.org/10.5194/bg-11-2147-2014, 2014.

Alberts, B., Johnson, A., Lewis, J., Raff, M., Roberts, K., and Walter, P.: Molecular Biology of the Cell, Garland Science, 4th edn., 2002.

Anderson, J. M. and Ingram, J. S. I.: Tropical Soil Biology and Fertility: A Handbook of Methods., CAB international, Wallingford, second edi edn., https://doi.org/10.2307/2261129, 1993.

Angst, G., Mueller, K. E., Nierop, K. G. J., and Simpson, M. J.: Plant- or microbial-derived? A review on the molecular composition of stabilized soil organic matter, Soil Biology and Biochemistry, 156, 108 189, https://doi.org/10.1016/j.soilbio.2021.108189, 2021.

Bettermann, A., Zethof, J. H. T., Babin, D., Cammeraat, E. L. H., Solé-Benet, A., Lázaro, R., Luna, L., Nesme, J., Sørensen, S. J., Kalbitz, K., Smalla, K., and Vogel, C.: Importance of microbial communities at the root-soil interface for extracellular polymeric substances and soil aggregation in semiarid grasslands, Soil Biology and Biochemistry, 159, 108 301, https://doi.org/10.1016/j.soilbio.2021.108301, 2021.

Blagodatsky, S. A. and Richter, O.: Microbial growth in soil and nitrogen turnover: a theoretical model considering the activity state of microorganisms, Soil Biology and Biochemistry, 30, 1743–1755, https://doi.org/10.1016/S0038-0717(98)00028-5, 1998.

Bossuyt, H., Denef, K., Six, J., Frey, S. D., Merckx, R., and Paustian, K.: Influence of microbial populations and residue quality on aggregate stability, Applied Soil Ecology, 16, 195–208, https://doi.org/10.1016/S0929-1393(00)00116-5, 2001.

Bucka, F. B., Kölbl, A., Uteau, D., Peth, S., and Kögel-Knabner, I.: Organic matter input determines structure development and aggregate formation in artificial soils, Geoderma, 354, 113 881–113 881, https://doi.org/10.1016/j.geoderma.2019.113881, 2019.

Bucka, F. B., Felde, V. J. M. N. L., Peth, S., and Kögel-Knabner, I.: Disentangling the effects of OM quality and soil texture on microbially mediated structure formation in artificial model soils, Geoderma, 403, 115 213, https://doi.org/10.1016/j.geoderma.2021.115213, 2021.

Campbell, E. E., Parton, W. J., Soong, J. L., Paustian, K., Hobbs, N. T., and Cotrufo, M. F.: Using litter chemistry controls on microbial processes to partition litter carbon fluxes with the Litter Decomposition and Leaching (LIDEL) model, Soil Biology & Biochemistry, 100, 160–174, https://doi.org/10.1016/j.soilbio.2016.06.007, 2016.

Castellano, M. J., Mueller, K. E., Olk, D. C., Sawyer, J. E., and Six, J.: Integrating plant litter quality, soil organic matter stabilization, and the carbon saturation concept, Global Change Biology, 21, 3200–3209, https://doi.org/10.1111/gcb.12982, 2015.

Christensen, B. T.: Physical fractionation of soil and structural and functional complexity in organic matter turnover, European Journal of Soil Science, 52, 345–353, https://doi.org/10.1046/j.1365-2389.2001.00417.x, 2001.

Cotrufo, M. F., Wallenstein, M. D., Boot, C. M., Denef, K., and Paul, E.: The Microbial Efficiency-Matrix Stabilization (MEMS) framework integrates plant litter decomposition with soil organic matter stabilization: do labile plant inputs form stable soil organic matter?, Global Change Biology, 19, 988–995, https://doi.org/10.1111/gcb.12113, 2013.

Crouzet, O., Consentino, L., Pétraud, J.-P., Marrauld, C., Aguer, J.-P., Bureau, S., Le Bourvellec, C., Touloumet, L., and Bérard, A.: Soil Photosynthetic Microbial Communities Mediate Aggregate Stability: Influence of Cropping Systems and Herbicide Use in an Agricultural Soil, Frontiers in Microbiology, 10, 1319, https://doi.org/10.3389/fmicb.2019.01319, 2019.

de Aguiar, T. C., de Oliveira Torchia, D. F., van Tol de Castro, T. A., Tavares, O. C. H., de Abreu Lopes, S., de Souza da Silva, L., Castro, R. N., Berbara, R. L. L., Pereira, M. G., and García, A. C.: Spectroscopic–chemometric modeling of 80 humic acids confirms the structural pattern identity of humified organic matter despite different formation environments, Science of The Total Environment, 833, 155 133, https://doi.org/10.1016/j.scitotenv.2022.155133, 2022.

Denef, K., Six, J., Bossuyt, H., Frey, S. D., Elliott, E. T., Merckx, R., and Paustian, K.: Influence of dry–wet cycles on the interrelationship between aggregate, particulate organic matter, and microbial community dynamics, Soil Biology and Biochemistry, 33, 1599–1611, https://doi.org/10.1016/S0038-0717(01)00076-1, 2001.

Dijkstra, P., Martinez, A., Thomas, S. C., Seymour, C. O., Wu, W., Dippold, M. A., Megonigal, J. P., Schwartz, E., and Hungate, B. A.: On maintenance and metabolisms in soil microbial communities, Plant and Soil, https://doi.org/10.1007/s11104-022-05382-9, 2022.

Gargulak, J. D., Lebo, S. E., and McNally, T. J.: Lignin, in: Kirk-Othmer Encyclopedia of Chemical Technology, pp. 1–26, John Wiley & Sons, Ltd, https://doi.org/10.1002/0471238961.12090714120914.a01.pub3, _eprint: https://onlinelibrary.wiley.com/doi/pdf/10.1002/0471238961.12090714120914.a01.pub3, 2015.

Gauch, H. G., Hwang, J. T. G., and Fick, G. W.: Model Evaluation by Comparison of Model-Based Predictions and Measured Values, Agronomy Journal, 95, 1442–1442, https://doi.org/10.2134/agronj2003.1442, 2003.

Georgiou, K., Jackson, R. B., Vindušková, O., Abramoff, R. Z., Ahlström, A., Feng, W., Harden, J. W., Pellegrini, A. F. A., Polley, H. W., Soong, J. L., Riley, W. J., and Torn, M. S.: Global stocks and capacity of mineral-associated soil organic carbon, Nature Communications, 13, 3797, https://doi.org/10.1038/s41467-022-31540-9, number: 1 Publisher: Nature Publishing Group, 2022.

Gurung, R. B., Ogle, S. M., Breidt, F. J., Williams, S. A., and Parton, W. J.: Bayesian calibration of the DayCent ecosystem model to simulate soil organic carbon dynamics and reduce model uncertainty, Geoderma, 376, 114 529, https://doi.org/10.1016/j.geoderma.2020.114529, 2020.

Hansen, S., Jensen, L. S., Nielsen, N. E., and Svendsen, H.: The Soil Plant System Model Daisy - Basic Principles and Modelling Approach, Copenhagen: The Royal Veterinary and Agricultural University., 1993.

Kallenbach, C. M., Frey, S. D., and Grandy, A. S.: Direct evidence for microbial-derived soil organic matter formation and its ecophysiological controls, Nature Communications, 7, 1–10, https://doi.org/10.1038/ncomms13630, 2016.

Kamolmanit, B., Vityakon, P., Kaewpradit, W., Cadisch, G., and Rasche, F.: Soil fungal communities and enzyme activities in a sandy, highly weathered tropical soil treated with biochemically contrasting organic inputs, Biology and Fertility of Soils, 49, 905–917, https://doi.org/10.1007/s00374-013-0785-7, 2013.

Kandeler, E., Tscherko, D., and Spiegel, H.: Long-term monitoring of microbial biomass, N mineralisation and enzyme activities of a Chernozem under different tillage management, Biology and Fertility of Soils, 28, 343–351, https://doi.org/10.1007/s003740050502, 1999.

Kopittke, P. M., Hernandez-Soriano, M. C., Dalal, R. C., Finn, D., Menzies, N. W., Hoeschen, C., and Mueller, C. W.: Nitrogen-rich microbial products provide new organo-mineral associations for the stabilization of soil organic matter, Global Change Biology, 24, 1762–1770, https://doi.org/10.1111/gcb.14009, 2018.

685 Kopittke, P. M., Dalal, R. C., Hoeschen, C., Li, C., Menzies, N. W., and Mueller, C. W.: Soil organic matter is stabilized by organo-mineral associations through two key processes: The role of the carbon to nitrogen ratio, Geoderma, 357, 113 974–113 974, https://doi.org/10.1016/j.geoderma.2019.113974, 2020.

Kpemoua, T. P. I., Barré, P., Chevallier, T., Houot, S., and Chenu, C.: Drivers of the amount of organic carbon protected inside soil aggregates estimated by crushing: A meta-analysis, Geoderma, 427, 116 089, https://doi.org/10.1016/j.geoderma.2022.116089, 2022.

690 Krause, L., Biesgen, D., Treder, A., Schweizer, S. A., Klumpp, E., Knief, C., and Siebers, N.: Initial microaggregate formation: Association of microorganisms to montmorillonite-goethite aggregates under wetting and drying cycles, Geoderma, 351, 250–260, https://doi.org/10.1016/j.geoderma.2019.05.001, 2019.

Kögel-Knabner, I., Guggenberger, G., Kleber, M., Kandeler, E., Kalbitz, K., Scheu, S., Eusterhues, K., and Leinweber, P.: Organo-mineral associations in temperate soils: Integrating biology, mineralogy, and organic matter chemistry, Journal of Plant Nutrition and Soil Science,
695 171, 61–82, https://doi.org/10.1002/jpln.200700048, 2008.

Laub, M., Demyan, M. S., Nkwain, Y. F., Blagodatsky, S., Kätterer, T., Piepho, H.-p., and Cadisch, G.: DRIFTS band areas as measured pool size proxy to reduce parameter uncertainty in soil organic matter models, Biogeosciences, 17, 1393–1413, https://doi.org/10.5194/bg-17-1393-2020, 2020.

Laub, M., Schlichenmeier, S., Vityakon, P., and Cadisch, G.: Litter Quality and Microbes Explain Aggregation Differences in a Tropical
700 Sandy Soil, Journal of Soil Science and Plant Nutrition, 22, 848–860, https://doi.org/10.1007/s42729-021-00696-6, 2022.

Lavallee, J. M., Conant, R. T., Paul, E. A., and Cotrufo, M. F.: Incorporation of shoot versus root-derived 13C and 15N into mineral-associated organic matter fractions: results of a soil slurry incubation with dual-labelled plant material, Biogeochemistry, 137, 379–393, https://doi.org/10.1007/s10533-018-0428-z, 2018.

Lavallee, J. M., Soong, J. L., and Cotrufo, M. F.: Conceptualizing soil organic matter into particulate and mineral-associated forms
705 to address global change in the 21st century, Global Change Biology, 26, 261–273, https://doi.org/10.1111/gcb.14859, _eprint: https://onlinelibrary.wiley.com/doi/pdf/10.1111/gcb.14859, 2020.

Loague, K. and Green, R. E.: Statistical and graphical methods for evaluating solute transport models: Overview and application, Journal of Contaminant Hydrology, 7, 51–73, https://doi.org/10.1016/0169-7722(91)90038-3, 1991.

Luo, Z., Baldock, J., and Wang, E.: Modelling the dynamic physical protection of soil organic carbon: Insights into carbon predictions and
710 explanation of the priming effect, Global Change Biology, 23, 5273–5283, https://doi.org/10.1111/gcb.13793, 2017.

Manzoni, S., Taylor, P., Richter, A., Porporato, A., and Ågren, G. I.: Environmental and stoichiometric controls on microbial carbon-use efficiency in soils, New Phytologist, 196, 79–91, https://doi.org/10.1111/j.1469-8137.2012.04225.x, 2012.

Marschmann, G. L., Pagel, H., Kügler, P., and Streck, T.: Equifinality, sloppiness, and emergent structures of mechanistic soil biogeochemical models, Environmental Modelling & Software, 122, 104 518, https://doi.org/10.1016/j.envsoft.2019.104518, 2019.

715 Necpálová, M., Anex, R. P., Fienen, M. N., Del Grosso, S. J., Castellano, M. J., Sawyer, J. E., Iqbal, J., Pantoja, J. L., and Barker, D. W.: Understanding the DayCent model: Calibration, sensitivity, and identifiability through inverse modeling, Environmental Modelling & Software, 66, 110–130, https://doi.org/10.1016/j.envsoft.2014.12.011, 2015.

Oldfield, E. E., Crowther, T. W., and Bradford, M. A.: Substrate identity and amount overwhelm temperature effects on soil carbon formation, Soil Biology and Biochemistry, 124, 218–226, https://doi.org/10.1016/j.soilbio.2018.06.014, 2018.

720 Puttaso, A., Vityakon, P., Saenjan, P., Trelo-ges, V., and Cadisch, G.: Relationship between residue quality, decomposition patterns, and soil organic matter accumulation in a tropical sandy soil after 13 years, Nutrient Cycling in Agroecosystems, 89, 159–174, https://doi.org/10.1007/s10705-010-9385-1, 2011.

Puttaso, A., Vityakon, P., Rasche, F., Saenjan, P., Treloges, V., and Cadisch, G.: Does Organic Residue Quality Influence Carbon Retention in a Tropical Sandy Soil?, Soil Science Society of America Journal, 77, 1001–1001, https://doi.org/10.2136/sssaj2012.0209, 2013.

725 R Core Team: R: A Language and Environment for Statistical Computing, https://www.r-project.org/, 2020.

Schrumpf, M., Kaiser, K., Guggenberger, G., Persson, T., Kögel-Knabner, I., and Schulze, E.-D.: Storage and stability of organic carbon in soils as related to depth, occlusion within aggregates, and attachment to minerals, Biogeosciences, 10, 1675–1691, https://doi.org/10.5194/bg-10-1675-2013, publisher: Copernicus GmbH, 2013.

Scrucca, L.: GA: A Package for Genetic Algorithms in R, Journal of Statistical Software, 53, 1–37, https://doi.org/10.18637/jss.v053.i04, 730 2013.

Segoli, M., De Gryze, S., Dou, F., Lee, J., Post, W., Denef, K., and Six, J.: AggModel: A soil organic matter model with measurable pools for use in incubation studies, Ecological Modelling, 263, 1–9, https://doi.org/10.1016/j.ecolmodel.2013.04.010, 2013.

Sinsabaugh, R. L., Manzoni, S., Moorhead, D. L., and Richter, A.: Carbon use efficiency of microbial communities: stoichiometry, methodology and modelling, Ecology Letters, 16, 930–939, https://doi.org/10.1111/ele.12113, 2013.

735 Sinsabaugh, R. L., Turner, B. L., Talbot, J. M., Waring, B. G., Powers, J. S., Kuske, C. R., Moorhead, D. L., and Follstad Shah, J. J.: Stoichiometry of microbial carbon use efficiency in soils, Ecological Monographs, 86, 172–189, https://doi.org/10.1890/15-2110.1, 2016.

Six, J. and Paustian, K.: Aggregate-associated soil organic matter as an ecosystem property and a measurement tool, Soil Biology & Biochemistry, 68, A4–A9, https://doi.org/10.1016/j.soilbio.2013.06.014, 2014.

Six, J., Elliott, E., and Paustian, K.: Soil macroaggregate turnover and microaggregate formation: a mechanism for C sequestration under 740 no-tillage agriculture, Soil Biology & Biochemistry, 32, 2099–2103, https://doi.org/10.1016/S0038-0717(00)00179-6, 2000.

Six, J., Feller, C., Denef, K., Ogle, S. M., Sa, J. C. d. M., and Albrecht, A.: Soil organic matter, biota and aggregation in temperate and tropical soils - Effects of no-tillage, Agronomie, 22, 755–775, https://doi.org/10.1051/agro:2002043, publisher: EDP Sciences, 2002.

Six, J., Frey, S. D., Thiet, R. K., and Batten, K. M.: Bacterial and Fungal Contributions to Carbon Sequestration in Agroecosystems, Soil Science Society of America Journal, 70, 555–569, https://doi.org/10.2136/sssaj2004.0347, _eprint: 745 https://acsess.onlinelibrary.wiley.com/doi/pdf/10.2136/sssaj2004.0347, 2006.

Soetaert, K., Petzoldt, T., and Setzer, R. W.: Solving Differential Equations in R: Package deSolve, Journal of Statistical Software, 33, 1–25, https://doi.org/10.18637/jss.v033.i09, 2010.

Tang, J. and Riley, W. J.: Weaker soil carbon–climate feedbacks resulting from microbial and abiotic interactions, Nature Climate Change, 5, 56–60, https://doi.org/10.1038/nclimate2438, 2015.

750 Tang, J. and Riley, W. J.: Competitor and substrate sizes and diffusion together define enzymatic depolymerization and microbial substrate uptake rates, Soil Biology and Biochemistry, 139, 107 624, https://doi.org/10.1016/j.soilbio.2019.107624, 2019.

Totsche, K. U., Amelung, W., Gerzabek, M. H., Guggenberger, G., Klumpp, E., Knief, C., Lehndorff, E., Mikutta, R., Peth, S., Prechtel, A., Ray, N., and Kögel-Knabner, I.: Microaggregates in soils, Journal of Plant Nutrition and Soil Science, pp. 1–33, https://doi.org/10.1002/jpln.201600451, 2017.

755 Van Soest, P. J. and Wine, R. H.: Determination of Lignin and Cellulose in Acid-Detergent Fiber with Permanganate, Journal of AOAC INTERNATIONAL, 51, 780–785, https://doi.org/10.1093/jaoac/51.4.780, 1968.

Vance, E., Brookes, P., and Jenkinson, D.: An extraction method for measuring soil microbial biomass C, Soil Biology & Biochemistry, 19, 703–707, https://doi.org/10.1016/0038-0717(87)90052-6, 1987.

Vityakon, P.: Degradation and restoration of sandy soils under different agricultural land uses in northeast Thailand: A review, Land Degradation and Development, https://doi.org/10.1002/ldr.798, 2007.

Vityakon, P., Meepech, S., Cadisch, G., and Toomsan, B.: Soil organic matter and nitrogen transformation mediated by plant residues of different qualities in sandy acid upland and paddy soils, NJAS - Wageningen Journal of Life Sciences, 48, 75–90, https://doi.org/10.1016/S1573-5214(00)80006-8, 2000.

Walkley, A. and Black, I. A.: An examination of the degtjareff method for determining soil organic matter, and a proposed modification of the chromic acid titration method, Soil Science, 37, 29–38, https://doi.org/10.1097/00010694-193401000-00003, 1934.

Wallach, D., Makowski, D., Jones, J. W., and Brun, F.: Chapter 8 - Parameter Estimation With Bayesian Methods, in: Working with Dynamic Crop Models (Third Edition), edited by Wallach, D., Makowski, D., Jones, J. W., and Brun, F., pp. 275–309, Academic Press, https://doi.org/10.1016/B978-0-12-811756-9.00008-3, 2019.

Wang, G., Post, W. M., and Mayes, M. A.: Development of microbial-enzyme-mediated decomposition model parameters through steady-state and dynamic analyses, Ecological Applications, 23, 255–272, https://doi.org/10.1890/12-0681.1, 2013.

Wang, G., Jagadamma, S., Mayes, M. A., Schadt, C. W., Megan Steinweg, J., Gu, L., and Post, W. M.: Microbial dormancy improves development and experimental validation of ecosystem model, The ISME Journal, 9, 226–237, https://doi.org/10.1038/ismej.2014.120, number: 1 Publisher: Nature Publishing Group, 2015.

Wang, S., Redmile-Gordon, M., Shahbaz, M., Ge, T., Zhang, M., Wu, Y., Liu, J., Huang, Q., and Cai, P.: Microbial formation and stabilisation of soil organic carbon is regulated by carbon substrate identity and mineral composition, Geoderma, 414, 115 762, https://doi.org/10.1016/j.geoderma.2022.115762, 2022.

Wieder, W. R., Grandy, A. S., Kallenbach, C. M., and Bonan, G. B.: Integrating microbial physiology and physio-chemical principles in soils with the MIcrobial-MIneral Carbon Stabilization (MIMICS) model, Biogeosciences, 11, 3899–3917, https://doi.org/10.5194/bg-11-3899-2014, 2014.

Yudina, A. and Kuzyakov, Y.: Saving the face of soil aggregates, Global Change Biology, 25, 3574–3577, https://doi.org/10.1111/gcb.14779, 2019.

Zech, S., Schweizer, S. A., Bucka, F. B., Ray, N., Kögel-Knabner, I., and Prechtel, A.: Explicit spatial modeling at the pore scale unravels the interplay of soil organic carbon storage and structure dynamics, Global Change Biology, 28, 4589–4604, https://doi.org/10.1111/gcb.16230, _eprint: https://onlinelibrary.wiley.com/doi/pdf/10.1111/gcb.16230, 2022.

Zhang, Y., Lavallee, J. M., Robertson, A. D., Even, R., Ogle, S. M., Paustian, K., and Cotrufo, M. F.: Simulating measurable ecosystem carbon and nitrogen dynamics with the mechanistically defined MEMS 2.0 model, Biogeosciences, 18, 3147–3171, https://doi.org/10.5194/bg-18-3147-2021, publisher: Copernicus GmbH, 2021.

Šimůnek, J., van Genuchten, M. T., and Šejna, M.: The HYDRUS-1D Software Package for Simulating the Movement of Water, Heat, and Multiple Solutes in Variably Saturated Media, Version 3.0, HYDRUS Software Series 1, Department of Environmental Sciences, University of California Riverside, Riverside, California, USA, 2005.